Supplementary information

Multiparameter characterisation of a nano-polypropylene representative test material with fractionation, light scattering, high-resolution microscopy, spectroscopy, and spectrometry methods

Dorota Bartczak[1], Aneta Sikora[1], Heidi Goenaga-Infante[1], Korinna Altmann[2], Roland Drexel[3], Florian Meier[3], Enrica Alasonati[4] Marc Lelong[4], Florence Cado [4], Carine Chivas-Joly [4], Marta Fadda[5], Alessio Sacco[5], Andrea Mario Rossi[5], Daniel Pröfrock[6], Dominik Wippermann[6], Francesco Barbero[7], Ivana Fenoglio[7], Andy M. Booth[8], Lisbet Sørensen[8,] Amaia Igartua[8], Charlotte Wouters[9], Jan Mast[9] , Marta Barbaresi[10], Francesca Rossi[11], Maurizio Piergiovanni[10], Monica Mattarozzi[10], Maria Careri[10], Thierry Caebergs[12], Anne-Sophie Piette[12], Jeremie Parot[13] and Andrea Mario Giovannozzi[5, *]

Table of contents

A. MD-AF4 Operating Conditions at LNE

LNE optimised parameters for AF4-UV-MALS: main parameters, separation field (cross-flow as a function of time), MALS and UV signal intensity.

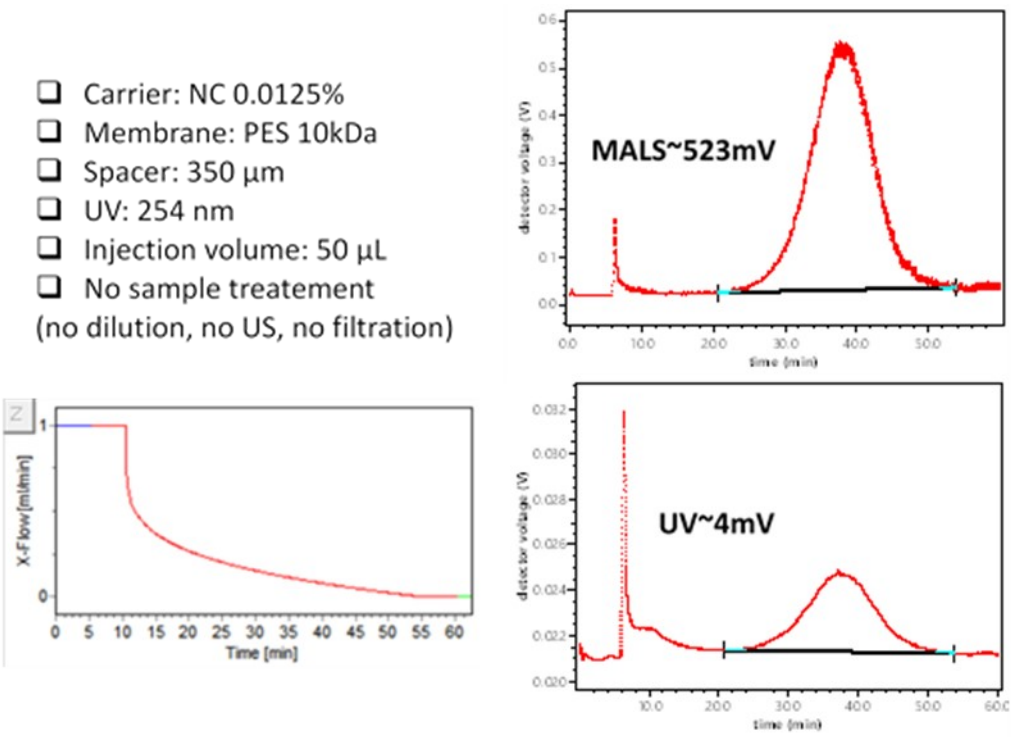

Figure 1. Optimised AF4-UV-MALS parameters and representative MALS and UV fractograms.

B. AF4-MALS Results per vial – Postnova

Two aliquots were taken from in total 12 vials, and each aliquot was fractionated in duplicate. For the cumulative distribution results' variations below 1.75% were obtained, with the largest variations on the largest size fraction. The R_g distribution averages for $R_{g,10}$, $R_{g,50}$ and $R_{g,90}$ are presented in Figure below. The run-to-run repeatability is visualized using error bars in the figure below, but the variations are very low and difficult to distinguish from the data points.

The MALS data analysis yielded for $R_{g,10}$ = 46.7 nm ± 0.6 nm, $R_{g,50}$ = 74.2 nm ± 0.8 nm and $R_{g,90}$ = 99.3 nm ± 1.75 nm.

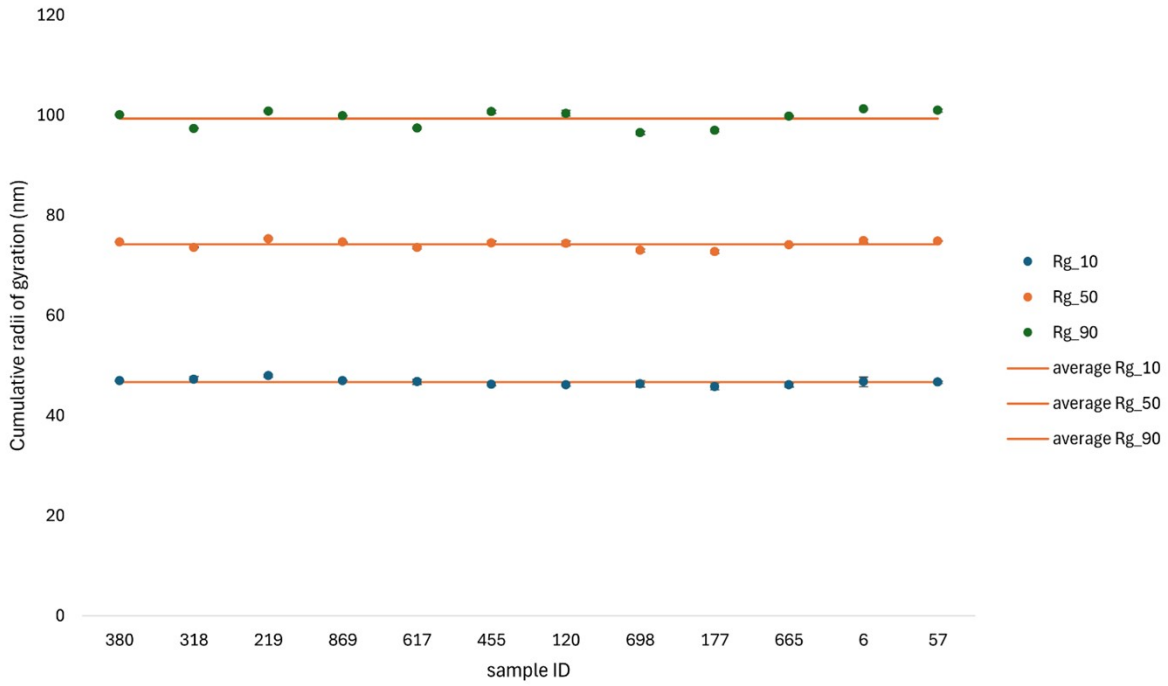

Figure 2. MALS results per vial.

The retention time in AF4 corresponds directly to the hydrodynamic size. After the determination of the effective channel height with polystyrene size standards (polystyrene beads 60 nm and 125 nm), the retention time can be translated to the hydrodynamic size distribution using the Stokes-Einstein-Equation. The so-determined effective channel height was checked by a fractionated monodisperse polystyrene 200 nm size standard, which was also used for quality control measurements. A hydrodynamic size distribution with cumulative results of $R_{h,10}$ = 66.2 nm ± 1.6 nm, $R_{h,50}$ = 98.2 nm ± 1.7 nm and $R_{h,90}$ = 130.9 nm ± 2.5 nm was derived. The calculations were based on the light scattering signal at 90°, which was also used to determine the weighted R_h results.

The Peak area under the MALS 90° signal can be used to estimate the particle number concentration. The angular dependent scattering is, among other parameters, proportional to the particle number concentration. The results show good agreement with the PTA results described in main text of the manuscript. Aliquot 318 showed a significantly lower particle concentration and

aliquot 455 a significantly larger particle concentration in PTA, both results are clearly identified and supported by MALS signals. But FFF-MALS was also able to detect smaller particle concentration variations between the vials. The diagram below displays the MALS peak area for different aliquots.

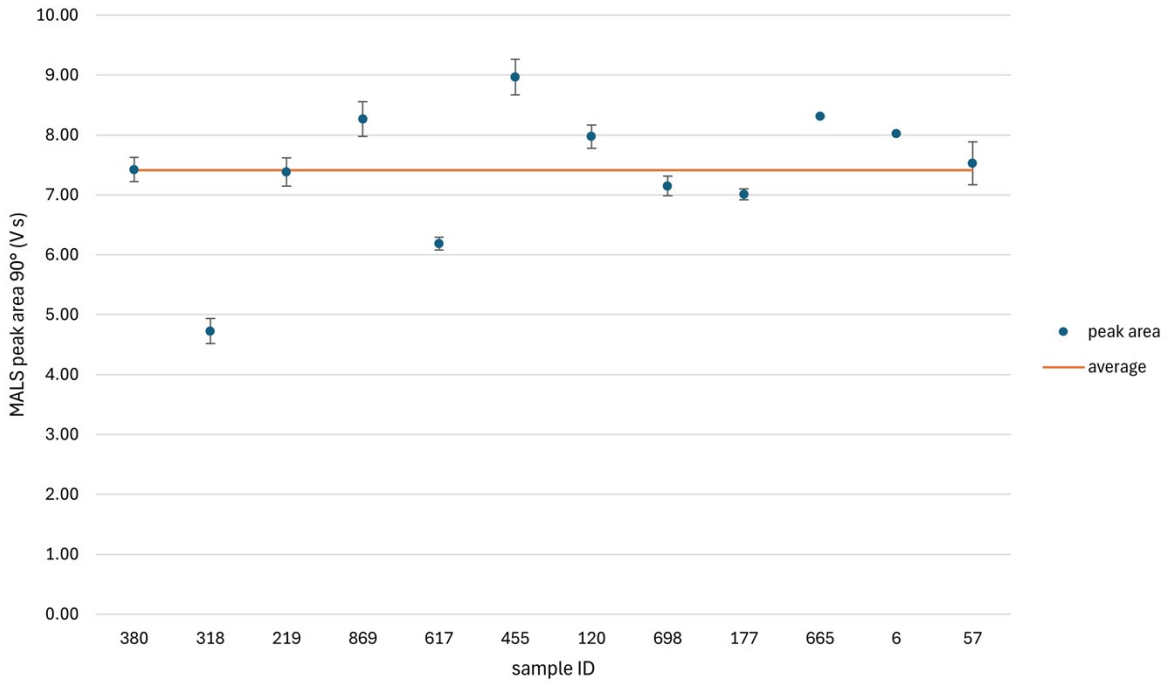

Figure 3. MALS peak area per vial.

C. AF4-MALS Results by SMD

Similar results to the ones reported in the text of the main manuscript were obtained by SMD, as shown in the Figure below.

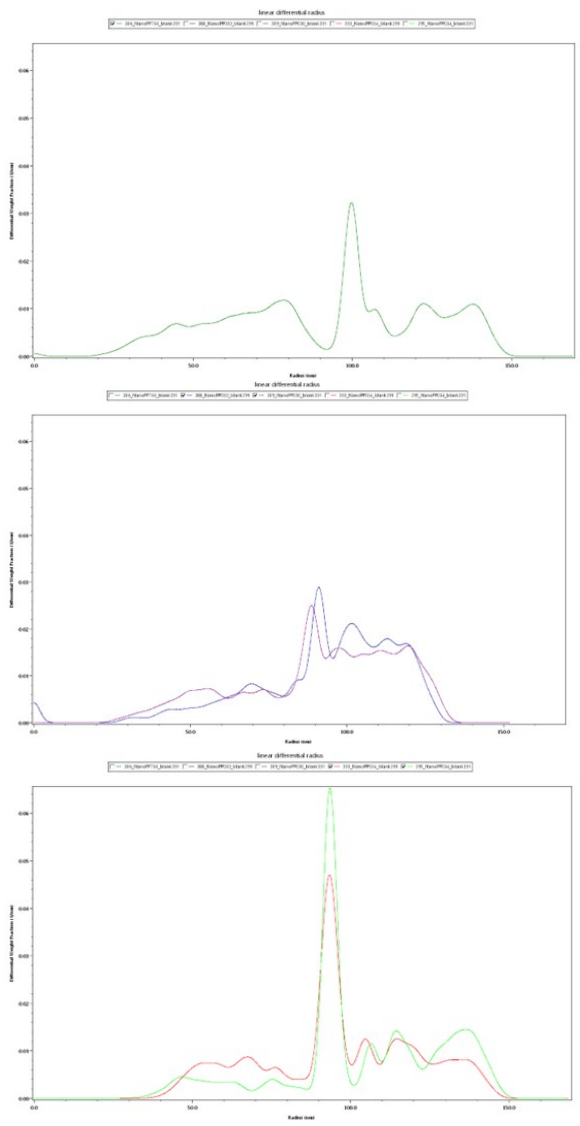

Figure 4. Representative AF4-MALS fractograms.

Size distribution obtained by AF4-MALS on three different vials (ID 766, ID 030, ID 034 which was freshly opened), within the same picture, the measurement is repeated for the latter two vials. Considering the weak signal and observing the same features for all vials, the results can be considered as repeatable and the sample to be homogenous among the vials. Inline DLS (not shown) was also performed. Because of the weak UV/Vis signal, and the need for the application of a baseline subtraction, some fluctuations can arise on quantities derived from the particle size distribution. It can be noticed that the mode information is less influenced by this feature, this is confirmed. Inline DLS shows slightly higher values.

Table 1. Summary of the obtained AF4/MALS and DLS results.

ID	Rec. (%)	R_geo,n	R_geo,w	R_geo,z	R_pk,z	D_FWHM_pk,DLS (sigma on FWHM peak)
766	104	55	92	111	100	236 (25)
030	115*	56	93	109	92	298 (25)
030	87	60	92	110	88	302 (38)
034	60	73	96	113	93	229 (15)
034	57	78	89	112	94	219 (16)

D. cFFF Results by Hereon

Measurement results for NanoPP using cFFF and MALS are in good agreement to each other. ID025 showed slightly higher radius compared to ID 130 and ID 662, whose results are close to each other. Standard deviation is at around 7 %.

Summary of the average (n = 4) R_g values obtained from MALS scattering data on three different vials, together with standard deviation are shown in a Table below.

Table 2. Summary of the obtained cFFF/MALS results.

Vial number	R_n / nm	Standard deviation nm	R_w / nm	Standard deviation / nm	R_z / nm	Standard deviation / nm
ID 025	73	5	75	6	77	7
ID 130	61	3	63	3	65	2
ID 662	61	7	64	5	66	5

E. Sciensano intra-lab validation study of 200 nm PS nanospheres (3200A) by TEM

1 Definitions and abbreviations

1.1 Definitions

Pixel size: the size of one pixel in an EM image (in nm).

Particle: minute piece of matter with defined physical boundaries[1].

Constituent particle: smallest indivisible unit of an agglomerate/aggregate[2].

Aggregate: particle comprising strongly bonded or fused particles where the resulting external surface area may be significantly smaller than the sum of calculated surface areas of the individual components[3].

Agglomerate: collection of weakly bound particles or aggregates or mixtures of the two where the resulting external surface area is similar to the sum of the surface areas of the individual components[3].

1.2 Abbreviations

AR: aspect ratio

C_m: mean measured value

C_{ref}: reference value

ECD: area-equivalent circle diameter

EM: electron microscopy

Fmin: minimum Feret diameter

NIST: National Institute of Standards and Technology

NM: nanomaterial

nm: nanometer

NP: nanoparticle

MICD: maximum inscribed circle diameter

PS: polystyrene

sd: Standard deviation

SOP: standard operating procedure

TEM: transmission electron microscopy

u_{cal}: uncertainty associated to calibration

$u_c(x)$: Combined uncertainty

U_{cx}: (Expanded) measurement uncertainty (k=2)

u_{day}: uncertainty due to day-to-day variation

u_{IP}: uncertainty associated to within-lab intermediate precision

u_r: uncertainty associated to repeatability

u_{tr}: uncertainty associated to trueness

Δm: = |reference value – mean measured value|

U_{Δ}: expanded uncertainty of the difference between the result and the certified value

2 Validation plan

2.1 Aim of the validation study

This intra-laboratory validation study aims to validate the measurement of a set of size and shape measurands of the constituent particles of polystyrene (PS) Nanosphere size standard 3200A by transmission electron microscopy (TEM). The objective is to determine the full uncertainty budget for the measurement of the mean, the mode and the percentiles (d10, d25, d50, d75, d90) of the number-based distributions of the minimum (Fmin) and maximum Feret diameters (Fmax), the area equivalent circle diameter (ECD), the maximum inscribed circle diameter (MICD) and the aspect ratio (AR).

2.2 Material

The material for which the method is validated is the Nanosphere size standard 3200A purchased from Thermo Fisher Scientific. They are part of a series of polymer micro/nanospheres with calibrated mean diameters traceable to the standard meter through the National Institute of Standards and Technology (NIST). According to the calibration certificate, the material has a certified/reference mean diameter of 202 ± 4 nm (k=2), as measured by TEM. The reported uncertainty is calculated from the observed variation in individual measurements taken (Random or Type A values) and possible sources of error in the system (Systematic or Type B values), following NIST Tech Note 1297[4].

2.3 Sample preparation

The vial is stored at 4°C before and after the specimen preparation. Before usage, the sample suspension is homogenized by vortex stirring for approximately 10-15 seconds. A dilution series with milliQ water is prepared and checked by TEM to determine the dilution factor which gives the optimal concentration of particles on the grid. TEM specimens are prepared using the grid-on-drop method[5] by bringing an Alcian blue pretreated pioloform- and carbon-coated, 400 mesh copper grid (Agar Scientific, Essex, England) on top of a drop of 10 µl of the dispersion. Grids are left in contact with the dispersion for 10 minutes. Afterwards, grids are blotted dry to remove excess sample and left to air-dry at room temperature. Grids are stored on a piece of filter paper in a petri-dish until TEM images are recorded.

2.4 Imaging

Images are taken using a calibrated[6] and well-aligned[7] Tecnai Spirit 12 TEM equipped with a Bottom-mounted 4X4K Eagle CCD camera (Thermo Fisher Scientific, Eindhoven, The Netherlands). The optimal imaging conditions will be determined and applied for each specimen. Images are recorded using the TEM imaging & analysis (TIA) software (Thermo Fisher Scientific). These SER- and EMI-formatted micrographs are converted to TIF format using the TIA software. The magnification of the micrographs and the number of particles/micrographs are determined such that the images are suitable for subsequent descriptive and quantitative image analyses.

2.5 Image analysis

Image analysis is performed with the ParticleSizer plugin[8] in ImageJ that uses different algorithms to measure constituent particle properties, depending on the type of particle (ellipsoidal or irregular) and type of overlap (none, touching, slightly overlapping, high or completely overlapping). These algorithms can be “Default”, “Irregular Watershed”, “Ellipse fitting” or “Single particle mode”. For application for regulatory use, each of these algorithms has been validated based on images of specific NM that belong to a certain “type of overlap” and “type of particle” combination.

It should be noted that in case of ellipse fitting, the Fmin and Fmax are taken to be the short and long axis of the fitted ellipse, respectively. In addition, in case of ellipe fitting the MICD is equal to the Fmin and should therefore not be reported separately.

2.6 Experimental design

The intermediate precision associated with the quantitative TEM measurement of the mean, mode and percentiles of the Fmin, Fmax, ECD, MICD and AR are estimated using a top-down approach. A total of 15 measurement repititions is done by performing three measurements per day on five different days (within a two weeks time frame). On each day, three TEM specimens are prepared from a new dilution of the same material vial and imaged by TEM. From each specimen, 10 images are recorded systematically and randomly over the grid surface. Each series of 10 images is analyzed using the ParticleSizer software. Figure 5 summarizes the experimental design of the top-down validation study.

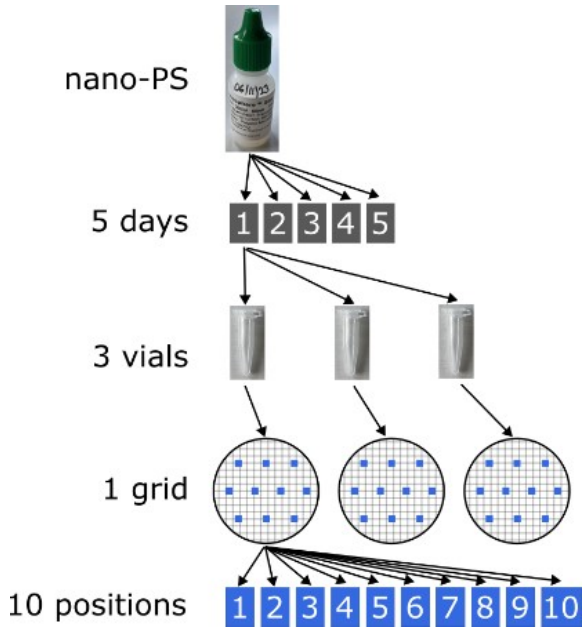

Figure 5. Experimental design of the top-down validation study for TEM analysis of the Nanosphere size standard.

2.7 SOPs

The methodology to characterize the selected materials consists of a combination of three SOPs: the NANoREG SOP on the 'Preparation of EM-grids containing a representative sample of a dispersed NM'[9], the NANoREG SOP on 'TEM imaging of nanomaterials'[10], and the NanoDefine SOP on 'Measurement of the minimal external dimension of the constituent particles of particulate materials from TEM images by the NanoDefine ParticleSizer software'[11].

2.8 Validation parameters

2.8.1 Homogeneity and stability

According to the manufacturer, the materials are suspended in concentrations optimized for colloidal stability. No further data on homogeneity and stability are available. Therefore, stability is evaluated visually based on the state of dispersion of the sample and in the TEM, by looking if no alterations occurred during the analysis time. The homogeneity is evaluated from the distribution of particles on the EM grid.

2.8.2 Working range

Limit of detection

In the TEM, the particle size detection limit is determined by the resolution of the microscope. A line resolution of 0.34 nm is claimed for the applied Tecnai G2 Spirit TEM with BioTwin lens configuration (FEI, Eindhoven, The Netherlands). This line resolution was confirmed by visualization of the [002] spacing of graphite of 0.335 nm.

The smallest detectable particle size is determined by the camera pixel size. A higher magnification and thus smaller pixel size allows detection of smaller particles, but comes at the cost of a reduced field of view and fewer particles per image. For example, at 18,500× magnification in our setup, the pixel size is 0.60 nm, which defines the resolution limit for particle detection.

To detect the particles, the image analysis software requires that the particles have enough contrast with the background in the TEM images. The mass-thickness contrast and the diffraction contrast depend on the thickness and atomic number of the particles. For crystalline materials, the contrast can also depend on particle orientation. However, since these are amorphous plastics, no such effect is expected.

Limit of quantification

The lower quantification limit is calculated based on the work of Merkus[12], who showed that large systematic deviations in size measurements can be avoided if the particle area of equi-axial particles consists of at least hundred pixels. Therefore, as a rule of thumb, the minimum Feret diameter detectable by the software is put at 10 pixels. The upper size quantification limit is restricted by the field of view and is set to one-tenth of the image size as proposed in ISO 13322-1[13].

Working range

The useful working range of the applied TEM and CCD camera configuration is defined by the lower and upper size quantification limits, and for any given magnification results in a factor of 40 (at a resolution of 4096x4096 pixels).

2.8.3 Selectivity

Selection of particles

To avoid subjectivity in the selection of particles by the microscopist, the SOP for TEM imaging[10] foresees that the micrographs were taken randomly and systematically, at 10 positions pre-defined by the microscope stage and evenly distributed over the entire grid area. When the field of view was not suitable e.g. because it was obscured by a grid bar or contained an artifact, the stage was moved sideways to the nearest suitable field of view. Micrographs of 10 regions on the grid were recorded with a 4*4 k Eagle CCD camera (Thermo Fisher Scientific, Eindhoven, the Netherlands) using the TEM imaging & analysis (TIA) software (Thermo Fisher Scientific, Eindhoven, The Netherlands).

Before particles are detected, the software creates a noise reduced and background subtracted image to avoid detecting contamination in the background. All particles that give enough contrast with the background are detected by the software. Incomplete particles on the border of images are rejected by the software, as their size and shape properties can’t be measured reliably.

Selectivity against other types of particles

The particles are first identified based on their gray value, and in second instance based on their general appearance including properties such as size and shape. Structures with clearly deviating size and shape are considered to be contaminant materials and should be omitted from analysis. Because the selected materials consist of nanoplastic particles suspended in an aqueous solution, it is expected that there will be no matrix substances present that would interfere with the detection and measurement of the particles.

2.8.4 Robustness

Robustness against the number of measured particles

The robustness of the method and the validation study is evaluated against variation in the number of measured particles by determining the uncertainty on the measurement of the relevant measurand in function of the number of analyzed particles based on subdatasets of measurements, following Wouters et al.[14].

Robustness against variations in the image analysis settings

Robustness against variations in the image analysis settings and variations of the image analysis mode used in the ParticleSizer plugin will be described.

2.8.5 Precision

The measurement precision associated with the quantitative TEM measurement of the size/shape measurands are estimated using a top-down approach as described in section 2.6.

The image analysis settings are optimized on a few images. The selected image analysis settings are then applied to the 15 sets of 10 images (each set originating from one TEM specimen, see Figure 1). Finally, 15 values for the measurand are obtained and used for the ANOVA. Data processing is performed using MS Excel.

The uncertainty associated to repeatability, u_r, and the uncertainty due to day-to-day variation, u_{day}, summarize the uncertainties related to the non-systematic variability in sample preparation, image acquisition, image analysis, and data analysis. u_r indicates the closeness of agreement between the results of measurements, taken over a short period, using the same instrument and taken by the same operator. u_{day} indicates the closeness of agreement between results originating from series of measurements taken by one laboratory and obtained over different days[15]. u_r and u_{day} are estimated via one-way analysis of variance, using following equations:

$$u_r = \frac{\sqrt{MS_{within}}}{C_m}$$

$$u_{day} = \begin{cases} \dfrac{\sqrt{\dfrac{MS_{between} - MS_{within}}{n_r}}}{C_m} & for\ MS_{between} > MS_{within} \\ \dfrac{\sqrt{\dfrac{MS_{within}}{n_r}}\sqrt[4]{\dfrac{2}{\nu_{MSwithin}}}}{C_m} & for\ MS_{between} < MS_{within} \end{cases}$$

with n_r the number of replicates per day (3 replicates), MS_{Within} the mean squares within days, $MS_{Between}$ the mean squares between days, $\nu_{MSwithin}$ is the number of degrees of freedom within sample units and C_m the mean.

The uncertainty associated to intermediate precision, $u_{IP,}$ combines the uncertainty associated to repeatability, u_r, and the uncertainty due to day-to-day variations, u_{day}:

$$u_{IP} = \sqrt{u_r^2 + u_{day}^2}$$

2.8.6 Uncertainty associated to calibration

The lower magnifications are calibrated using the cross-grating method and the higher magnifications are calibrated using the image shift method based on a 2160 lines/mm optical diffraction-cross grating (Agar Scientific, Stansted, England). The calibration method is implemented following ASTM E766

guidelines and by using the magnification calibration software which is integrated in the Tecnai user interface software (Thermo Fisher Scientific, Eindhoven, The Netherlands)[16].

The most recent values of the uncertainty related to calibration, based on the variation of calibration values over time, are summarized in Table 3. These values are used for all size measurands. Since the aspect ratio is calculated as Fmax/Fmin, u_{cal} for the aspect ratio is calculated from u_{cal} for Fmax and Fmin using the appropriate error propagation rules.

Table 3. Uncertainties associated to calibration (u_{cal}) as a function of the selected TEM magnification.

Magnification	u_{cal} (%)
440x	1.03
690x	0.92
890x	0.93
1200x	0.95
1400x	0.87
1900x	0.83
2900x	0.80
4800x	0.81
6800x	0.83
9300x	0.87
11000x	0.87
13000x	0.99
18500x	1.02
23000x	0.78
30000x	0.09
49000x	0.10
68000x	0.14
98000x	0.26
120000x	0.41
150000x	0.41
180000x	0.72

2.8.7 Uncertainty associated to trueness

The uncertainty associated to trueness (u_{tr}) is obtained by combining u_{IP} with the uncertainty associated to trueness of a certified reference material ($u_{tr,ref}$). Although the material under study is not certified, it is provided with a reported uncertainty for the particle size determined by TEM. Therefore, this reported uncertainty will be used as $u_{tr,ref}$ for all considered size parameters, since it is the best available option. Because the aspect ratio is calculated as Fmax/Fmin, $u_{tr,ref}$ for the aspect ratio is calculated from $u_{tr,ref}$ for Fmax and Fmin using the appropriate error propagation rules.

To obtain the uncertainty associated to trueness (u_{tr}), the uncertainty associated to trueness of the reference material is combined with u_{IP} as follows:

$$u_{tr} = \sqrt{u_{tr,ref}^2 + u_{IP}^2}$$

2.8.8 Combined and expanded measurement uncertainty

The uncertainty contributions explained above are to be combined in the method's full uncertainty budget. u_r and u_{day} are type A uncertainties, which are derived from repeated testing. They cover all sources of variation between analyses and the typical between-day variation. u_{cal} and u_{tr} are type B uncertainty components (e.g. values taken from certificates and expert judgement). If one assumes that all the uncertainty contributions for the quantitative TEM method are covered by the uncertainty associated to repeatability, the uncertainty due to day-to-day variation, the uncertainty associated to calibration and the uncertainty associated to trueness, then the combined measurement uncertainty, $u_c(x)$, can be estimated from:

$$u_c(x) = \sqrt{u_{IP}^2 + u_{cal}^2 + u_{tr}^2}$$

The uncertainties are combined using the normal root-sum-square manner, resulting in the combined measurement uncertainty $u_c(x)$. When assuming that the combined uncertainty is normally distributed and a confidence level of approximately 95% is required, the combined uncertainty can be multiplied by a coverage factor of 2 to obtain the expanded measurement uncertainty, U_{cx}[17]. Table 4 provides a template to summarize the different uncertainty contributions to the combined and expanded measurement uncertainties, for e.g. the measurements of the median Feret min diameter.

Table 4. Summary table of the different uncertainty contributions to the combined and expanded measurement uncertainties, for the median Feret min diameter.

Median Feret Min.	
Mean: C_m	nm
Standard deviation: *sd*	nm
Uncertainty associated to repeatability: u_r	%
Uncertainty due to day-to-day variation: u_{day}	%
Uncertainty associated to intermediate precision: u_{IP}	%
Uncertainty associated to calibration: u_{cal}	%
Uncertainty associated to trueness: u_{tr}	%
Combined uncertainty: $u_c(x)$	%
Measurement uncertainty (k = 2): U_{cx}	%

2.8.9 Trueness

To assess the trueness of the described methodology, a comparison of the outcome with the certified size value is required. For this material, a reference size value is reported, however, it does not meet the requirements of a accredited certified reference material. Therefore, we can get an idea on the trueness of our approach but a real quality control of the trueness of our approach is not possible. To check whether the measurement result is in agreement with the reference value, the absolute difference between the mean measured value C_m and the reference value C_{ref} is calculated $\Delta_m = |C_m - C_{ref}|$. If Δ_m is smaller than the expanded uncertainty of the difference between the result and the reference value, $U_\Delta = 2\sqrt{u_c^2 + u_{ref}^2}$ (k=2, expressed in nm), then there is no significant difference between the measurement and the reference value[18]. Otherwise, the results are significantly biased.

For measurands where no certified or reference values are available, the trueness cannot be assessed.

2.9 Reporting

A validation report will be prepared, containing the results of the intra-lab validation and discussing all aspects of the validation plan.

3 Validation report

3.1 Scope of the validation study

This validation study covers the use of transmission electron microscopy (TEM) for determining the particle size and shape of particles in the polystyrene size standard 3200A. The scope includes evaluation of trueness, precision, and total measurement uncertainty using a reference material with a reported size value of 202 nm determined by TEM. The combined and expanded measurement uncertainty on the measurement of the mean, the mode and the percentiles (d10, d25, d50, d75, d90) of the number-based distributions of the minimum (Fmin) and maximum Feret diamters (Fmax), the area equivalent circle diameter (ECD), the maximum inscribed circle diameter (MICD) and the aspect ratio (AR) will be reported. Other material properties, such as chemical composition, are not within the scope of this study. The outcome of this study is believed to be transferrable to other electron microscopy imaging systems operating under comparable conditions.

3.2 Material

The vial of Nanosphere size standard 3200A (batch number 3200-045, packaging lot #260104) was purchased from Thermo Fisher Scientific. The reference mean diameter of 202 ± 4 nm (k=2) of the product was obtained using TEM by the producer.

3.3 Sample preparation

The analysis of the dilution series showed that a dilution factor of 10x was optimal. Sample preparation was done as described as in section 2.3 of the validation plan and in line with the SOP on preparation of EM-grids[9].

3.4 Imaging

The SOP on TEM imaging of NM[10] is applied to obtain representative EM micrographs of nanomaterials coated on TEM grids. The optimized TEM imaging conditions are presented in Table 5.

Table 5. Summary of the TEM imaging conditions applied.

TEM imaging conditions	
Type of TEM	Tecnai Spirit 12
Type of analysis	TEM
CCD camera	Bottom-mounted 4X4K Eagle CCD camera
Resolution (pixels)	4096 x 4096
Number of images	10
Magnification	SA 4800
Pixel size (nm)	2.24
Spot size	3
Emission step	1
Objective aperture	3

Date of the last maintenance of TEM	25/02/2022
Date of the last calibration of TEM	16/05/2022
Calibration method	the cross-grating method based on a 2160 lines/mm optical diffraction-cross grating (Sigma, Brussels, Belgium)

3.5 Image analysis

The ellipse fitting mode of the ParticleSizer is applied for the image analysis since it performed best in separating and defining the borders of individual particles within agglomerates (Figure 6). Artefacts and wrongly detected particles (e.g. multiple overlapping particles detected as one) were manually omitted. In case of ellipse fitting, the Fmin and Fmax are equal to the short and long axis of the fitted ellipse, respectively. In addition, the MICD is equal to the Fmin and is therefore not reported separately. The construction of number-based particle size and shape distributions and statistical analysis is done in Python (Figure 7). The mode of the distributions is determined based on the kernel density estimates.

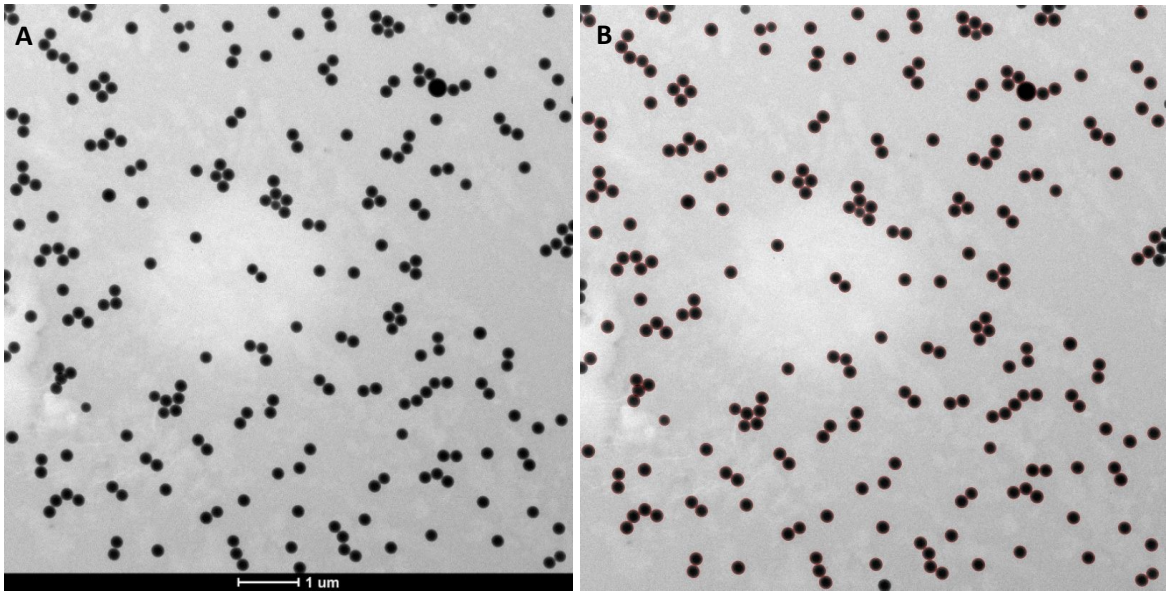

Figure 6. Representative TEM micrograph of sample W'71A of material 3200A (A) and annotated micrograph resulting from the image analysis (B). Red outlines indicate borders of detected particles.

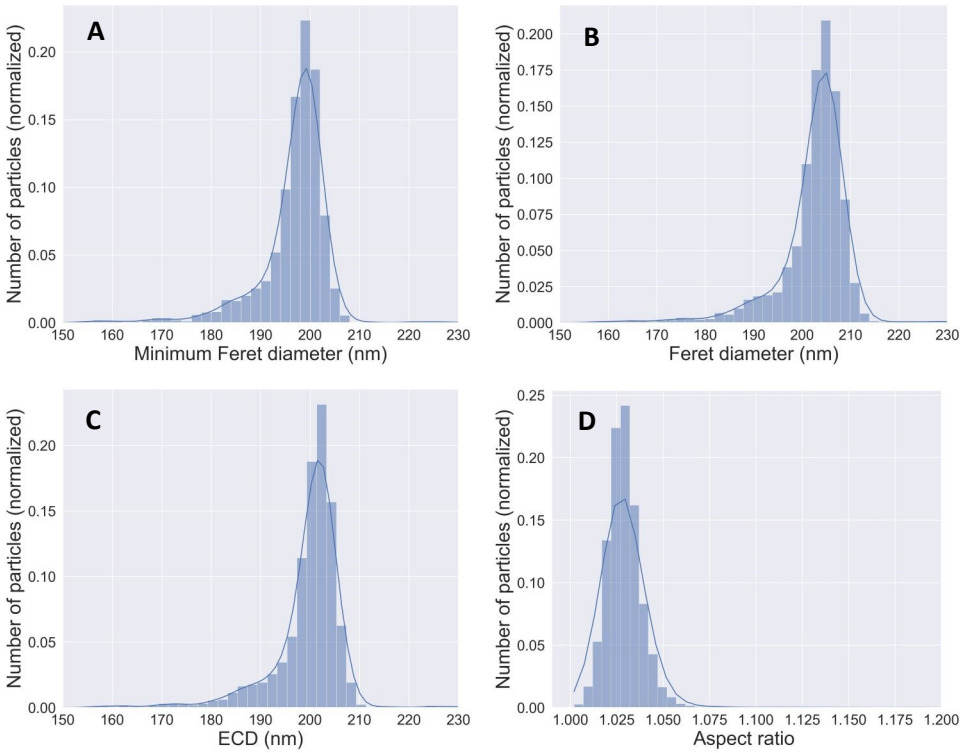

Figure 7. Normalized number-based distribution and kernel density estimation of the Fmin (A), Fmax (B), ECD (C) and AR (D) of the constituent particles detected in a series of 10 images of sample W'71A.

3.6 Experimental design

The measurement precision associated with the quantitative TEM measurement of the mean, mode and percentiles of the Fmin, Fmax, ECD and AR are estimated using a top-down approach, as described in section 2.6 of the validation plan. An overview of the prepared samples and the timeline of the different steps in the validation plan are presented in Table 6.

Table 6. General overview of the samples and the timing of different experimental steps.

Sciensano's Reference	Product Reference	Batch Reference	Received	Opened	Sampled	Imaging	Image analyis
W'71A	3200A	3200-045	20/06/2023	28/11/2023	28/11/2023	28/11/2023	19/12/2023
W'71B	3200A	3200-045	20/06/2023	28/11/2023	28/11/2023	28/11/2023	19/12/2023
W'71C	3200A	3200-045	20/06/2023	28/11/2023	28/11/2023	28/11/2023	19/12/2023
W'72A	3200A	3200-045	20/06/2023	28/11/2023	29/11/2023	29/11/2023	19/12/2023
W'72B	3200A	3200-045	20/06/2023	28/11/2023	29/11/2023	29/11/2023	19/12/2023
W'72C	3200A	3200-045	20/06/2023	28/11/2023	29/11/2023	29/11/2023	21/12/2023
W'75A	3200A	3200-045	20/06/2023	28/11/2023	04/12/2023	04/12/2023	02/01/2024
W'75B	3200A	3200-045	20/06/2023	28/11/2023	04/12/2023	04/12/2023	02/01/2024
W'75C	3200A	3200-045	20/06/2023	28/11/2023	04/12/2023	04/12/2023	11/01/2024
W'76A	3200A	3200-045	20/06/2023	28/11/2023	06/12/2023	06/12/2023	02/01/2024
W'76B	3200A	3200-045	20/06/2023	28/11/2023	06/12/2023	06/12/2023	02/01/2024
W'76C	3200A	3200-045	20/06/2023	28/11/2023	06/12/2023	06/12/2023	02/01/2024
W'77A	3200A	3200-045	20/06/2023	28/11/2023	07/12/2023	07/12/2023	02/01/2024

W'77B	3200A	3200-045	20/06/2023	28/11/2023	07/12/2023	07/12/2023	02/01/2024
W'77C	3200A	3200-045	20/06/2023	28/11/2023	07/12/2023	07/12/2023	02/01/2024

3.7 Validation parameters

3.7.1 Homogeneity and stability

No report on the stability or homogeneity of the material was available from the manufacturer.

Based on a visual inspection of the dispersion, no alterations in stability could be observed during the period of the validation study. No precipitation of particles was observed. During analysis time in the electron microscope no alterations to the particles could be observed.

To evaluate the homogeneity of the suspension, multiple areas on the EM grid were checked in terms of the distribution of particles on the grid. Variations in the particle concentration can be observed (Figure 8), and in regions with higher concentration, more agglomeration of particles is observed.

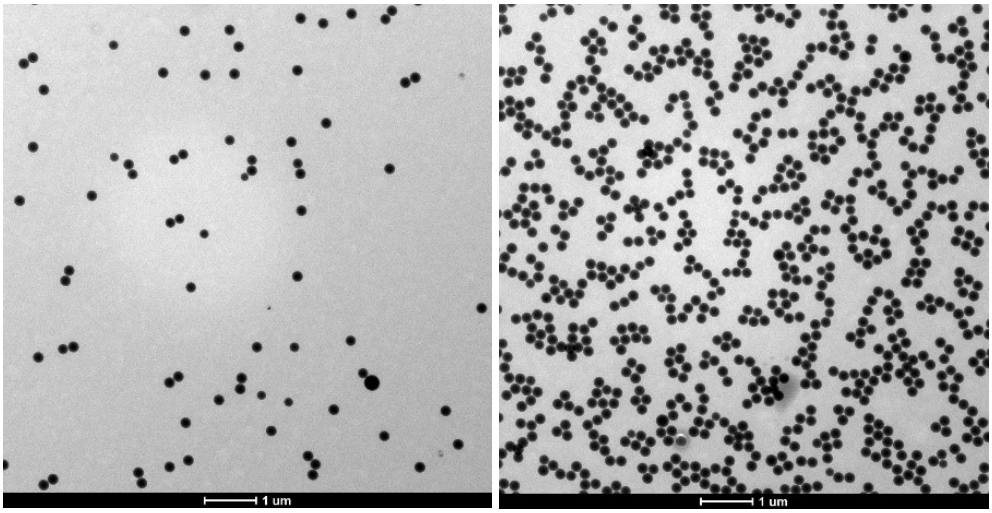

Figure 8. TEM images from selected locations on the grid to show variations in the particle distribution.

3.7.2 Working range

Limit of detection

For the given microscope and camera configuration, the applied magnification of 4800x results in micrographs with a pixel size of 2.24 nm, which forms the limit of detection.

To detect the particles, the image analysis software requires that the particles have enough contrast with the background in the TEM images. For 3200A, the contrast between the PS particles and the background is high enough for their detection.

Limit of quantification

The lower quantification limit is calculated based on the work of Merkus[12] and is therefore set at 10 pixels. Given the pixel size of 2.24 nm at a magnification of 4800 times, the limit of quantification is 22.4 nm. 100% of the particles have an Fmin larger than this value. The upper size quantification limit is restricted by the field of view and is set to one-tenth of the image size as proposed in ISO 13322-1[13]. At a magnification of 4800 times, the upper size quantification limit is 918 nm. 100% of the particles have an Fmax smaller than this value.

Working range

The useful working range of the applied TEM and CCD camera configuration is defined by the lower and upper size quantification limits, and for any given magnification results in a factor of 40 given the resolution of 4096x4096 pixels. For a magnification of 4800 times, the useful working range ranges from 22.4 nm to 918 nm.

3.7.3 Selectivity

Selection of particles

To avoid subjectivity in the selection of particles by the microscopist, the SOP for TEM imaging foresees that the micrographs were taken randomly and systematically, at 10 positions pre-defined by the microscope stage and evenly distributed over the entire grid area. When the field of view was not suitable e.g. because it was obscured by a grid bar or contained an artifact, the stage was moved sideways to the nearest suitable field of view. Micrographs of 10 regions on the grid were recorded with a 4*4 k Eagle CCD camera (Thermo Fisher Scientific) using the TEM imaging & analysis (TIA) software (Thermo Fisher Scientific). The given magnification of 4800 times results in micrographs with a field of view of 9175 nm by 9175 nm.

Before particles are detected, the software creates a noise reduced and background subtracted image to avoid detecting contamination in the background. All particles that give enough contrast with the background are detected by the software. Incomplete particles on the border of images are rejected by the software.

Selectivity against other types of particles

Particles were identified based on their gray value, and constituent particles were selected from all detected particles based on their general appearance including properties such as size and shape. The selected materials consist of nanoplastics suspended in an aqueous solution; there were no matrix substances present that interfered with the detection and measurement of the particles.

3.7.4 Robustness

Robustness against the number of measured particles

The robustness of the method and the validation study is evaluated against variation in the number of measured particles by determining the uncertainty related to particle number (U_N), the intermediate precision (U_{IP}) and the expanded uncertainty (U_{cx}) on the measurement of the relevant measurand in function of the number of analyzed particles based on sub datasets of measurements, as explained in Wouters et al.[14]

U_N with a confidence level of 95% steadily decreases as a function of particle number for all percentiles, as shown in Figure 5. The uncertainty calculation is here shown for the ECD, but takes on similar values for the other size parameters. For d25, d50, d75 and d90, U_N is below 1% for N>79 and does not decrease much more for increasing N. Hence, increasing the number of particles over 79 will not have a strong effect on the precision related to particle number. For d10, a stronger dependency on the number of particles is observed. This is a consequence of the shape of the particle size distribution, which has a tail on the side of the lower percentiles. As a result, more particles need to be measured to reach the same precision on d10 as on the other percentiles. For the minimum number of particles we measured per data set, i.e. 500, U_N lies around 1% for d10. This is only a small fraction compared to the overall uncertainty of 4.8%. An increase in the number of particles above 500 will only lead to a small decrease in U_N and thus will not be of significant influence. Decreasing the number of particles below 500, causes a strong increase in U_N on d10, and thus might have an influence on the precision obtained in the validation study.

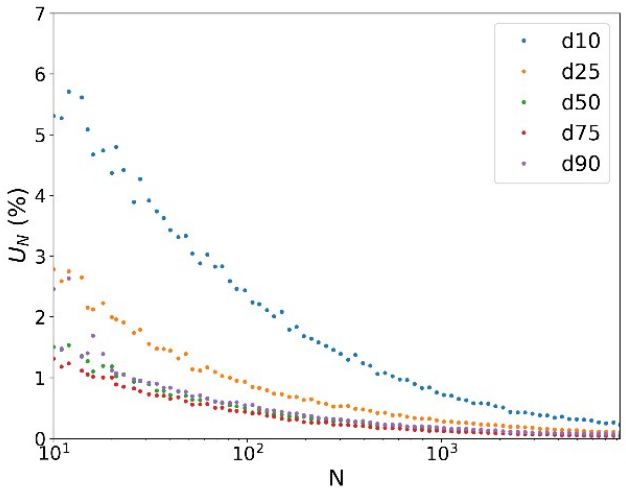

Figure 9. U_N as a function of number of measured particles for the different percentiles of the ECD.

Figure 10 presents the uncertainties U_N, U_{IP} and U_{cx} (all calculated at k = 2, corresponding to a 95% confidence interval) on the d50 of the ECD as a function of number of particles, plotted on a log-log scale. As the particle count increases, U_N steadily decreases, approaching zero, indicating the expected statistical reduction in uncertainty with larger sample sizes. In contrast, both U_{IP} and U_{cx} exhibit much slower declines, with the rate of decrease diminishing as N increases. Increasing the number of measured particles thus has a marginal effect on the overall uncertainty which is capped off around 4 % at N = 39.

Similar trends were observed for other ECD percentiles. For instance, the uncertainties for d10, d25, d75 and d90 also levelled off, with approximate cap values of 6%, 5%, 4%, 4% at N=100, N=36, N=37, N=29, respectively. These results highlight that while increasing particle count initially reduces measurement uncertainty, there exists a practical limit beyond which additional measurements yield very limited returns in uncertainty reduction.

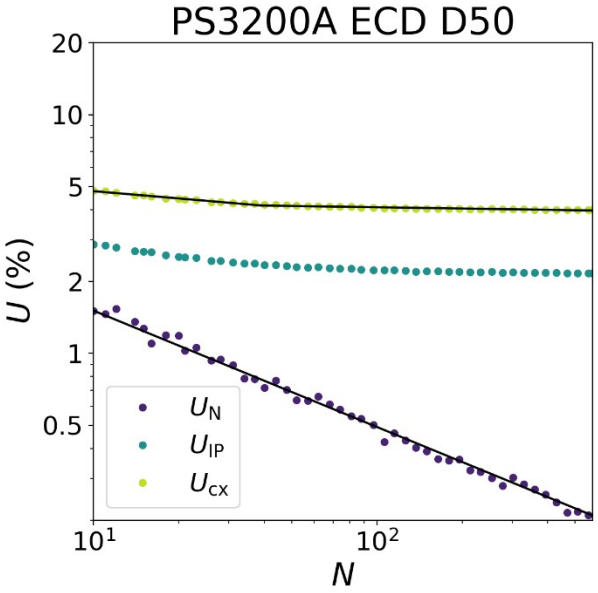

Figure 10. U_N, U_{IP} and U_{cx} on the d50 of the ECD as a function of number of particles.

Robustness against variations in the image analysis settings

In general, the method is quite robust in small changes in the image analysis parameters since all PS particles have convenient circular projected shape and provide a distinct contrast with respect to the background and are easily distinguished from background or artefacts.

Changing the image analysis mode to 'Default mode', results in a worse identification of the borders of overlapping particles within agglomerates (Figure 11), since the borders are just defined by the watershed algorithm and don't take into account the expected shape of the particle. Because there is quite a strong degree of agglomeration of particles within these samples, the choice of analysis mode can be expected to influence the outcome of the analysis and the validation study, especially for the Fmin, ECD and AR parameters, which depend more strongly on the particle shape.

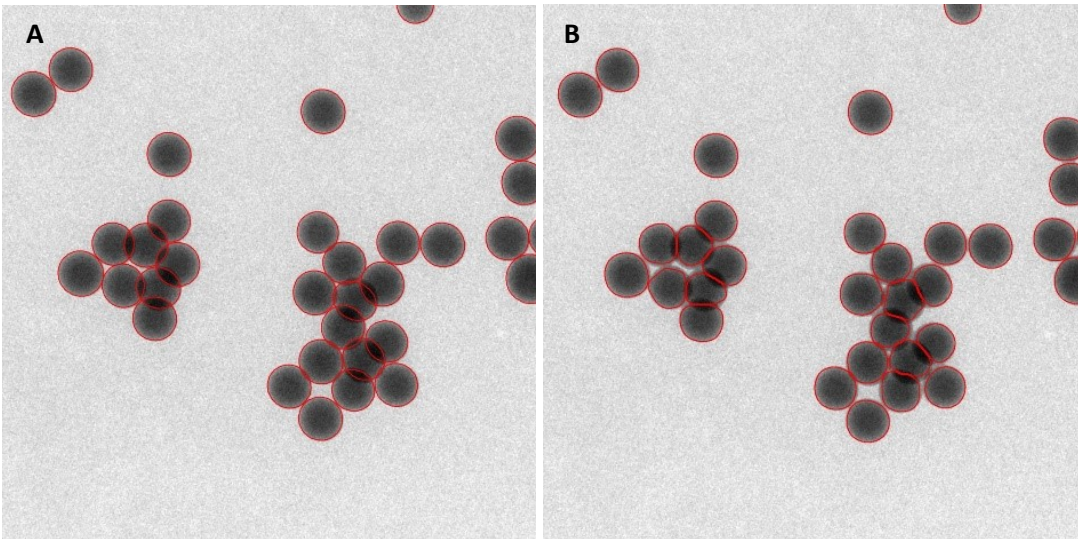

Figure 11. Results of the analysis in 'Ellipse fitting mode' (A) versus 'Default mode' (B) illustrated on a few agglomerates of PS 3200A.

For our analysis, wrongly detected particles within agglomerates and artefacts were removed from the analysis manually. To check whether this has an influence on the outcome of the validation study, the analysis of one dataset (W'75A) with relatively strong degree of agglomeration was repeated without removing erroneously detected particles. An ANOVA test was done on the resulting datasets to check for significant differences. We find that the outcome depends on the measurand. For Fmax, which will be the most strongly affected by the combined detection of multiple particles within agglomerates, the p-value of the resulting ANOVA test gives 0.03 (<0.05) hence the two datasets are significantly different. However, for a more robust measurand like the ECD, the outcome of the anova is p=0.4 (>0.05) and in this case the two datasets can be assumed equal.

3.7.5 Precision

Table 5-Table 8 show the precision of the particle measurement of the mean, mode and percentiles of the Feret min, Feret max, ECD and Aspect ratio of 3200A estimated by the uncertainty associated to intermediate precision (u_{IP}), combining the uncertainty associated to repeatability (u_r) and the uncertainty due to day-to-day variation (u_{day}) of the quantitative TEM approach.

3.7.6 Uncertainty associated to calibration

The uncertainty associated to the calibration of the TEM for a magnification of 4800 times corresponds to a value of 0.8%. This value is used for all size measurands. Since the aspect ratio is calculated as Fmax/Fmin, u_{cal} for the aspect ratio is calculated from u_{cal} for Fmax and Fmin using the appropriate error propagation rules and results in 1.1%.

3.7.7 Uncertainty associated to trueness

The uncertainty associated to trueness (u_{tr}) is determined as described in section 2.8.7 of the validation plan. Only a reference measurement value is available for the mean ECD of 3200A. It is assumed that the trueness uncertainty of other size parameters is in line with the trueness uncertainty of the reference material of the mean ECD ($u_{tr,ref}$=1%). Since the aspect ratio is calculated as Fmax/Fmin, $u_{tr,ref}$ for the aspect ratio is calculated from $u_{tr,ref}$ for Fmax and Fmin using the appropriate error propagation rules and results in 1.4%. The $u_{tr,ref}$ value is combined with u_{IP} as described in section 2.8.7 of the validation plan to obtain the uncertainty associated to trueness, resulting in the values given in Table 5-Table 8.

3.7.8 Combined and expanded measurement uncertainty

The uncertainty contributions explained above are combined in the method's full uncertainty budget. Table 7-Table 10 summarize the uncertainties associated to the repeatability, day-to day variation, intermediate precision, calibration and trueness contributing to the combined ($u_c(x)$) and expanded (U_{cx}) measurement uncertainties, for the measurements of the mean, mode and percentiles of the Fmin, Fmax, ECD and aspect ratio.

Table 7. Relative uncertainties of the TEM measurement of the mean, median (d50) and other percentile values (d10, d25, d75, d90) of the minimum Feret diameter of PS 3200A.

Fmin	Mean	Mode	d10	d25	d50	d75	d90
C_m (nm)	195	197	187	192	196	199	201
sd (nm)	2	2	3	3	2	2	2
u_r	0.8%	0.6%	1.3%	1.2%	0.8%	0.6%	0.6%
u_{day}	0.7%	0.7%	0.8%	0.9%	0.8%	0.7%	0.6%
u_{IP}	1.1%	1.0%	1.5%	1.5%	1.1%	0.9%	0.9%
u_{cal}	0.8%	0.8%	0.8%	0.8%	0.8%	0.8%	0.8%
u_{tr}	1.3%	1.2%	1.7%	1.6%	1.3%	1.2%	1.2%
$u_c(x)^A$	2.0%	1.9%	2.5%	2.5%	2.0%	1.8%	1.8%
U_{cx}^B	3.9%	3.7%	5.0%	5.1%	4.0%	3.6%	3.6%

[A] Combined measurement uncertainties, k=1 (68%).

[B] Expanded measurement uncertainties, k=2 (95%).

Table 8. Relative uncertainties of the TEM measurement of the mean, median (d50) and other percentile values (d10, d25, d75, d90) of the (maximum) Feret diameter of PS 3200A.

Fmax	Mean	Mode	d10	d25	d50	d75	d90
C_m (nm)	201	202	192	198	202	205	207
sd (nm)	2	2	3	3	2	2	2
u_r	0.8%	0.6%	1.4%	1.3%	0.8%	0.7%	0.6%
u_{day}	0.7%	0.6%	0.8%	0.9%	0.7%	0.6%	0.6%
u_{IP}	1.0%	0.9%	1.6%	1.6%	1.1%	0.9%	0.9%
u_{cal}	0.8%	0.8%	0.8%	0.8%	0.8%	0.8%	0.8%
u_{tr}	1.3%	1.2%	1.8%	1.7%	1.3%	1.2%	1.2%
$u_c(x)^A$	1.9%	1.8%	2.5%	2.5%	2.0%	1.8%	1.8%
U_{cx}^B	3.9%	3.6%	5.1%	5.1%	4.0%	3.6%	3.6%

[A] Combined measurement uncertainties, k=1 (68%).

[B] Expanded measurement uncertainties, k=2 (95%).

Table 9. Relative uncertainties of the TEM measurement of the mean, median (d50) and other percentile values (d10, d25, d75, d90) of the Area-equivalent circle diameter of PS 3200A.

ECD	Mean	Mode	d10	d25	d50	d75	d90
C_m (nm)	198	200	190	195	199	202	204
sd (nm)	2	2	3	3	2	2	2
u_r	0.8%	0.7%	1.3%	1.2%	0.8%	0.6%	0.6%
u_{day}	0.7%	0.8%	0.7%	0.9%	0.7%	0.6%	0.6%
u_{IP}	1.0%	1.0%	1.5%	1.5%	1.1%	0.9%	0.9%
u_{cal}	0.8%	0.8%	0.8%	0.8%	0.8%	0.8%	0.8%
u_{tr}	1.3%	1.2%	1.7%	1.7%	1.3%	1.2%	1.2%
$u_c(x)^A$	1.9%	1.9%	2.5%	2.5%	2.0%	1.8%	1.8%
U_{cx}^B	3.9%	3.8%	5.0%	5.1%	4.1%	3.6%	3.6%

[A] Combined measurement uncertainties, k=1 (68%).

[B] Expanded measurement uncertainties, k=2 (95%).

Table 10. Relative uncertainties of the TEM measurement of the mean, median (d50) and other percentile values (d10, d25, d75, d90) of the Aspect ratio of PS 3200A.

AR	Mean	Mode	d10	d25	d50	d75	d90
C_m (nm)	1.029	1.027	1.019	1.024	1.029	1.035	1.042
sd (nm)	0.008	0.007	0.0009	0.0006	0.0009	0.001	0.002
u_r	0.8%	0.7%	0.08%	0.03%	0.03%	0.06%	0.1%
u_{day}	0.3%	0.1%	0.04%	0.05%	0.08%	0.1%	0.1%
u_{IP}	0.9%	0.7%	0.09%	0.05%	0.09%	0.1%	0.2%
u_{cal}	1.1%	1.1%	1.1%	1.1%	1.1%	1.1%	1.1%
u_{tr}	1.6%	1.6%	1.4%	1.4%	1.4%	1.4%	1.4%
$u_c(x)^A$	2.2%	2.1%	1.8%	1.8%	1.8%	1.8%	1.8%
U_{cx}^B	4.2%	4.2%	3.6%	3.6%	3.6%	3.6%	3.6%

[A] Combined measurement uncertainties, k=1 (68%).

[B] Expanded measurement uncertainties, k=2 (95%).

3.7.9 Trueness

To assess the trueness of our approach, a comparison with the certified or reference size value is required[18]. Based on information of the manufacturer, we could assume that the mean certified diameter of the material is the most equivalent to the mean ECD. The mean ECD measured by our approach is 198 ± 7 nm and the reference value reported is 202 ± 4 nm. The difference between both values is Δ_m= 4 nm, which is smaller than the expanded uncertainty of the difference between the result and the reference value of 8 nm. This means our result is in agreement with the measured reference value.

However, we can not make a final conclusion on the trueness of our approach. Since this material is not officially accredited as reference material with exact information missing on the uncertainty determination and it is not exactly the same measurement parameter that is being compared (ECD vs. diameter in unspecified orientation), it is not suitable to do a proper comparison and assess the trueness of our approach.

3.8 Conclusion

Material stability was pertained throughout the validation study and a sufficient homogeneous distribution of particles on the grid was achieved. The Ellipse fitting mode of the ParticleSizer plugin allows detecting most of the constituent particles correctly, and it was shown that removing the wrongly detected particles had no significant impact. The validation study shows that our approach of sample preparation, TEM imaging and analysis of the 3200A material gives precise characterization results. The intermediate precision obtained is similar for all size parameters. It ranges from 0.9% to 1.6% with the highest values corresponding to the d10 percentile and the lowest values to the d75 or d90 perecentiles due to left skewedness of the size histograms. For the AR, the intermediate precision is below 1% for all measurands. For almost all parameters, the uncertainty associated to repeatability, u_r is larger than uncertainty associated to day-to-day variation, u_{day}. For the median Fmin, Fmax, ECD and AR parameters the mean value corresponds respectively to 196 nm, 202 nm, 199 nm and 1.029 with expanded uncertainties of 4.0%, 4.0%, 4.1% and 3.6%. Based on a comparison of the reference value (202±4 nm) and our measurement value for the mean ECD (198±7 nm), our measurement is accurate.

4 Dilution series of 3200A to determine limit of detection and quantification

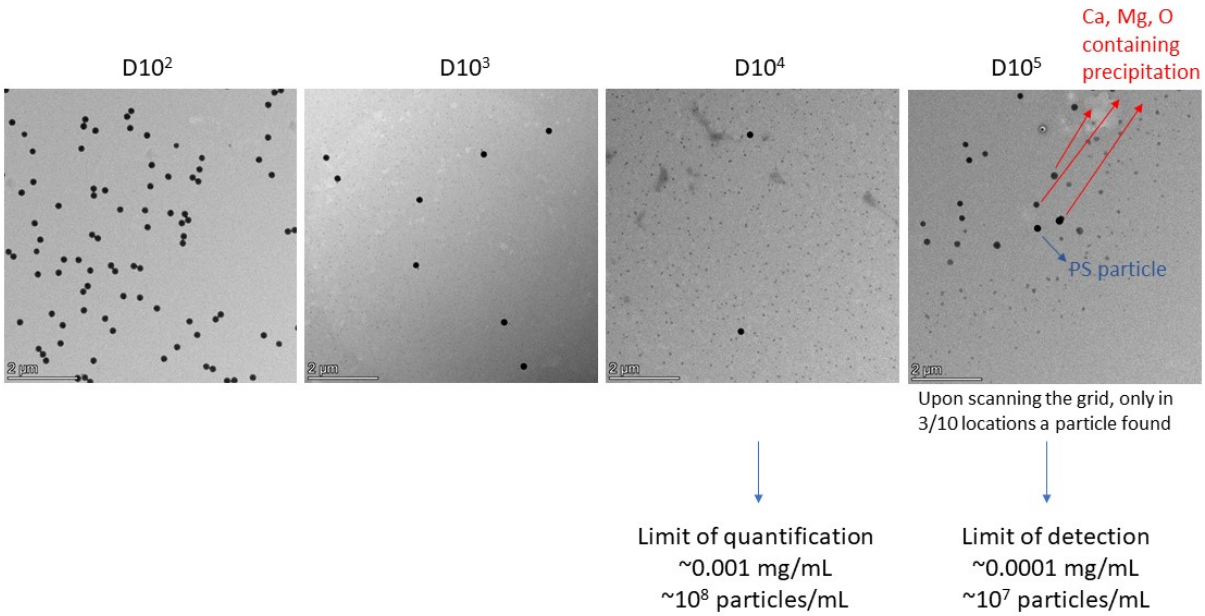

Figure 12. Representative TEM images of different dilutions of PS 3200A particles in bottled drinking water. The limit of detection was established at ~10^7 particles/mL, and the limit of quantification, defined as the concentration at which sufficient particles could be detected to generate a reliable size distribution (average 2 particles per image), at ~10^8 particles/mL. At the highest dilution (image on the right), precipitated particles containing Ca, Mg and O, resulting from the minerals present in the bottled water, are visible on the grid. Due to the similar morphology, they can potentially interfere with PS identification. However, these precipitates could be simply removed by washing the grid two times with ultrapure water.

5 References

1. ISO. *Cleanrooms and Associated Controlled Environments - Part 6: Vocabulary. ISO 14644-6:2007* (2007).

2. Rauscher, H., Kestens, V., Rasmussen, K., Linsinger, T. & Stefaniak, E. Guidance on the implementation of the Commission Recommendation 2022/C 229/01 on the definition of nanomaterial. *JRC Publications Repository* https://publications.jrc.ec.europa.eu/repository/handle/JRC132102 (2023) doi:10.2760/143118.
3. ISO. *Nanotechnologies - Terminology and Definitions for Nano-Objects - Nanoparticle, Nanofibre and Nanoplate*. *ISO/TS 27687:2008* (2008).
4. Taylor, B. N. & Kuyatt, C. E. Guidelines for Evaluating and Expressing the Uncertainty of NIST Measurement Results. NIST Technical Note 1297. (1994).
5. Mast, J., Verleysen, E. & De Temmerman, P.-J. Physical Characterization of Nanomaterials in Dispersion by Transmission Electron Microscopy in a Regulatory Framework. in *Advanced Transmission Electron Microscopy* (eds. Deepak, F. L., Mayoral, A. & Arenal, R.) 249–270 (Springer International Publishing, Cham, 2015). doi:10.1007/978-3-319-15177-9_8.
6. ISO. *Microbeam Analysis - Analytical Electron Microscopy - Methods for Calibrating Image Magnification by Using Reference Materials with Periodic Structures*. *ISO 29301:2017* (2017).
7. Rodenburg, J. M. Understanding transmission electron microcsope alignment: a tutorial. *Microscopy and Analysis* **18**, 3 (2004).
8. Wagner, T. https://imagej.net/ParticleSizer and https://zenodo.org/record/820296#.XAZ9XttKi00. (2016).
9. Mast, J. *et al.* NANoREG D2.10 SOP 01 Preparation of EM-grids containing a representative sample of a dispersed NM. (2015).
10. Mast, J. *et al.* NANoREG D2.10 SOP 02 Transmission electron microscopic imaging of nanomaterials. (2015).
11. European Commission *et al. The NanoDefine Methods Manual: Part 3 Standard Operating Procedures (SOPs)*. (Publications Office of the European Union, 2020).
12. Merkus, H. G. *Particle Size Measurements: Fundamentals, Practice, Quality*. (Springer, Pijnacker, 2009).
13. International Organization for Standardization. *ISO 13322-1, Particle Size Analysis-Image Analysis Methods*. (2014).
14. Wouters, C., Kestens, V., Verleysen, E. & Mast, J. Assessing particle count in electron microscopy measurements of nanomaterials to support regulatory guidance. *Sci Rep* **15**, 11803 (2025).
15. Roebben, G. *et al.* Reference materials and representative test materials: the nanotechnology case. *Journal of Nanoparticle Research* **15**, 1455 (2013).
16. ASTM. Standard Practice for Calibrating the Magnification of a Scanning Electron Microscope. *ASTM INTERNATIONAL* 6 (2014) doi:10.1520/E0766.
17. ISO. *Uncertainty of Measurement - Part 3: Guide to the Expression of Uncertainty in Measurement (GUM:1995)*. *ISO/IEC GUIDE 98-3:2008* (2008).
18. Linsinger, T. P. J. Application Note 1: Comparison of a measurement result with the certified value. (2010).

F. TEM and STEM-EDX of nanoPP samples by Sciensano

TEM data - including TEM and HAADF-STEM images, spectral maps, and EDX spectra - are presented for particles detected on grids prepared by various methods. Background signals in the EDX spectra, such as carbon from the support film, oxygen from ambient contamination, and silicon and copper from X-ray fluorescence (induced in the detector and grid components by primary X-rays emitted from the sample), are unavoidable. These background contributions may result in peaks for these elements; however, such signals are typically not specific to the particles themselves. In certain cases, however, a clearly elevated signal compared to the background (visible in the spectral images) indicates that these elements (e.g., C, Cu, Si, respectively) can be attributed to the particle(s). For example, an increased carbon signal can form an indication that the particle might be plastic, although this alone does not confirm its composition.

1. Grid-on-drop deposition (10’ contact)

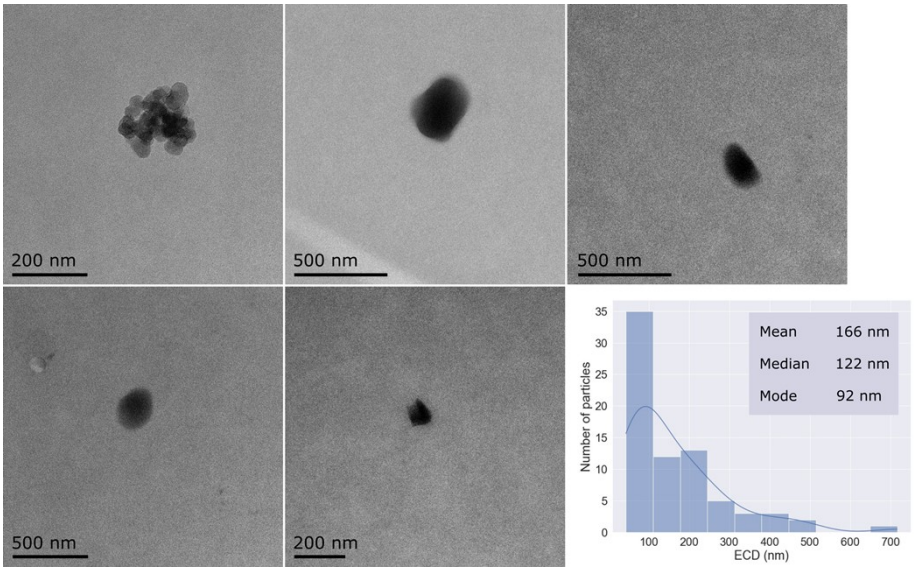

Figure 13. TEM images of particles detected in nano-PP sample prepared by grid-on-drop deposition and size histogram of the manually measured area-equivalent circular diameter (ECD) values.

The particle size distribution measured by TEM (Figure 13) of the subfraction of particles assumed to be nano-PP (as analyzed on a subset by STEM-EDX) is based on a limited number of 74 particles. The low statistics can be related to the limit of detection of the TEM-based approach. TEM analysis of a dilution series of dispersions of near-spherical PS nanoplastics of 200 nm showed that particle number concentrations below 10^8 particles/ml can not be reliably identified and characterized (Electronic supplementary information, section E.4). For polydisperse materials, like the examined nanoPP, this detection limit might be considerably higher. Conversion of the PP mass concentrations given in Table 5 of the original manuscript to number concentrations results roughly in $2*10^9$ particles/ml, given a particle diameter of 150 nm and density of 0.9 g/cm^3, which is on the limit of quantification for TEM-based methods. This likely explains the limited number of particles that could be included in the size distribution.

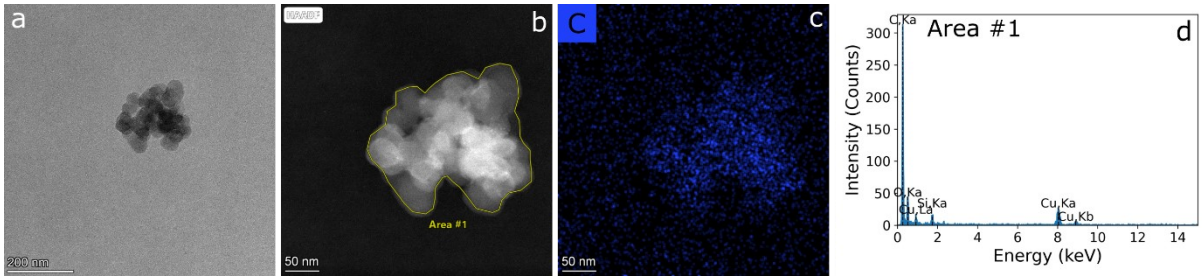

Figure 14. TEM image of aggregated/agglomerated particles (a). HAADF-STEM image of the same particles (b). EDX analysis shows that the particle contains an elevated C content compared to the background, with the spectral image of C (c) and the EDX spectrum of the area #1 (d), as indicated in b.

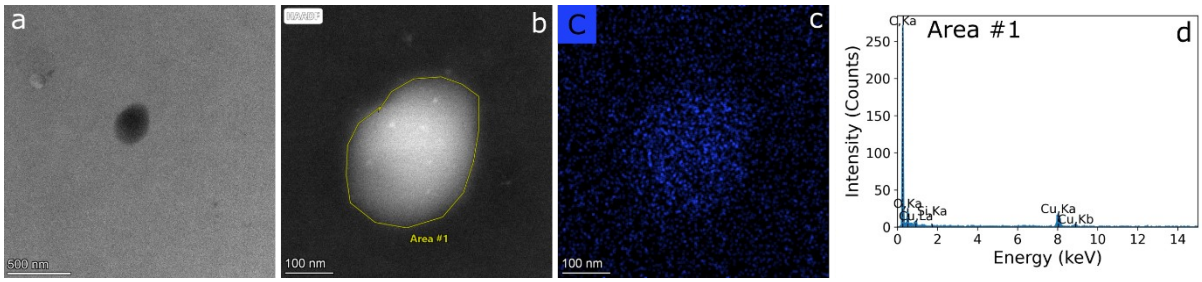

Figure 15. TEM image of an isolated particle (a). HAADF-STEM image of the same particle (b). EDX analysis shows that the particle contains an elevated C content compared to the background, with the spectral image of C (c) and the EDX spectrum of the area #1 (d), as indicated in b.

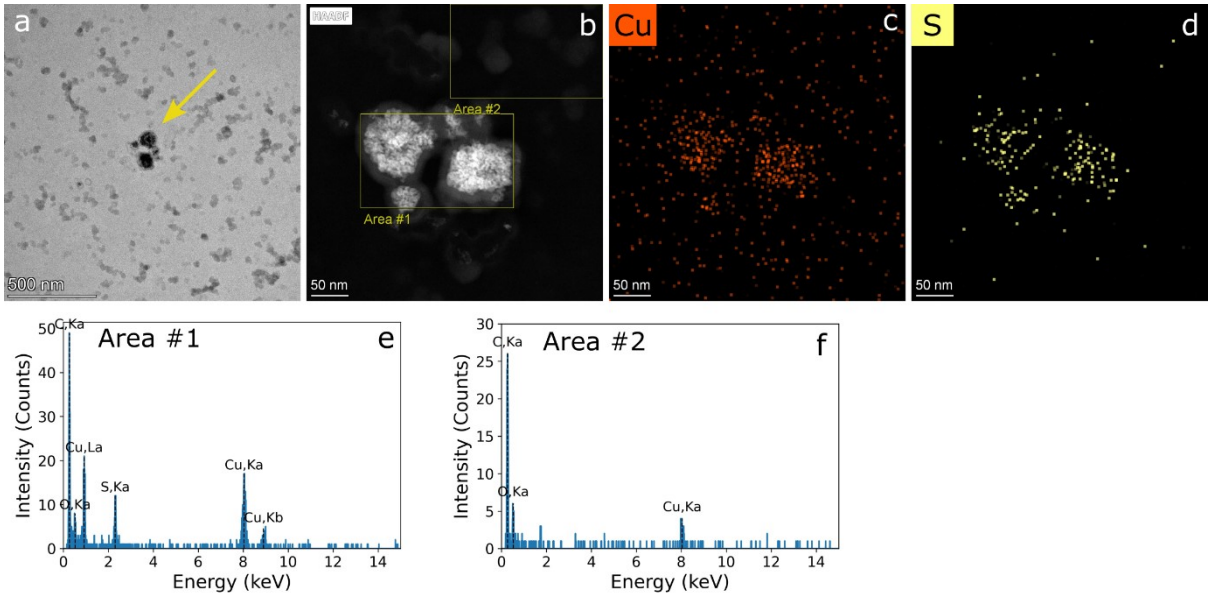

Figure 16. TEM image of a group of particles, indicated by a yellow arrow. The speckles in the background are due to instabilities in the C film (a). HAADF-STEM image of the indicated particles (rotated view) (b). EDX analysis shows that the particles contain an elevated Cu and S content compared to the background, with the spectral image of Cu (c) and S (d), and the EDX spectrum of the area #1 (e) and area #2 (f), indicated by the rectangles in b.

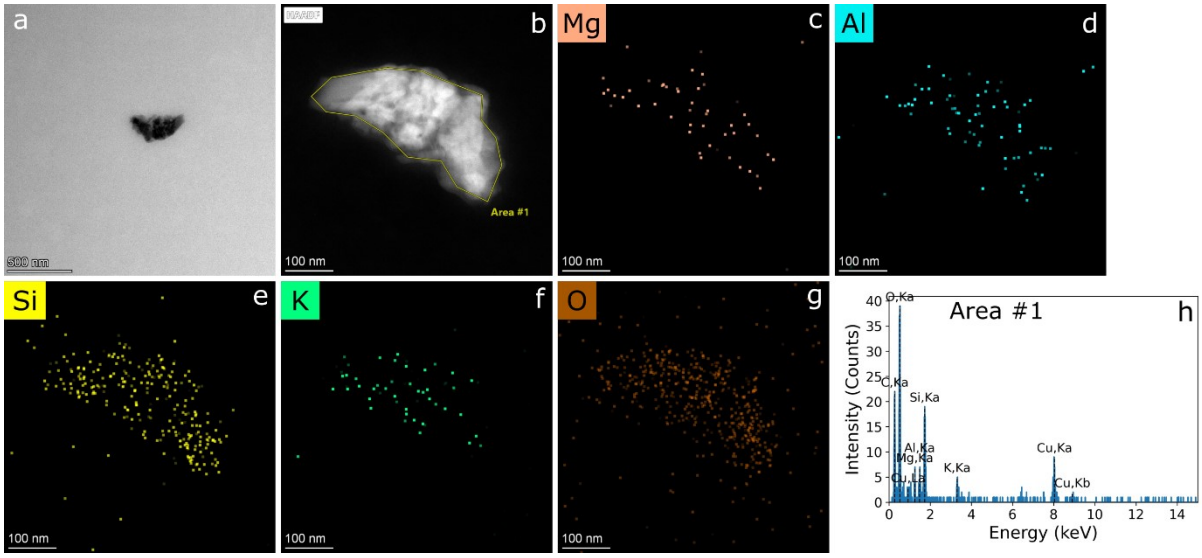

Figure 17. TEM image of an isolated particle (a). HAADF-STEM image of the same particle (rotated view) (b). EDX analysis shows that the particle contains Mg, Al, Si, K and O, with the spectral image of Mg (c), Al (d), Si (e), K (f) and O (g) and the EDX spectrum of the area #1 (h), as indicated in b.

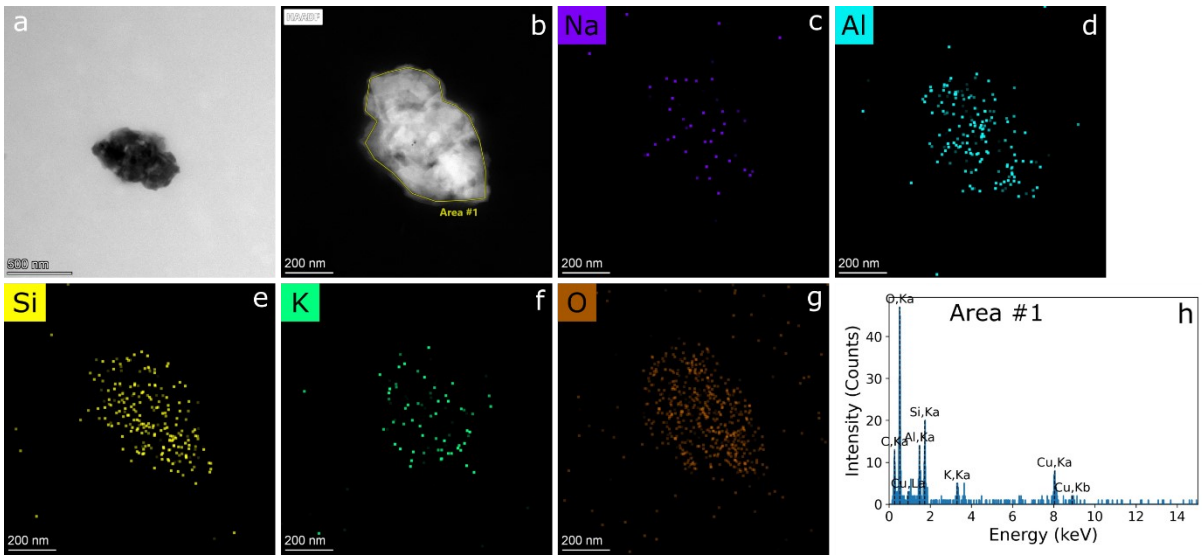

Figure 18. TEM image of an isolated particle (a). HAADF-STEM image of the same particle (rotated view) (b). EDX analysis shows that the particle contains Na, Al, Si, K and O, with the spectral image of Na (c), Al (d), Si (e), K (f) and O (g) and the EDX spectrum of the area #1 (h), as indicated in b.

2. On-grid centrifugation

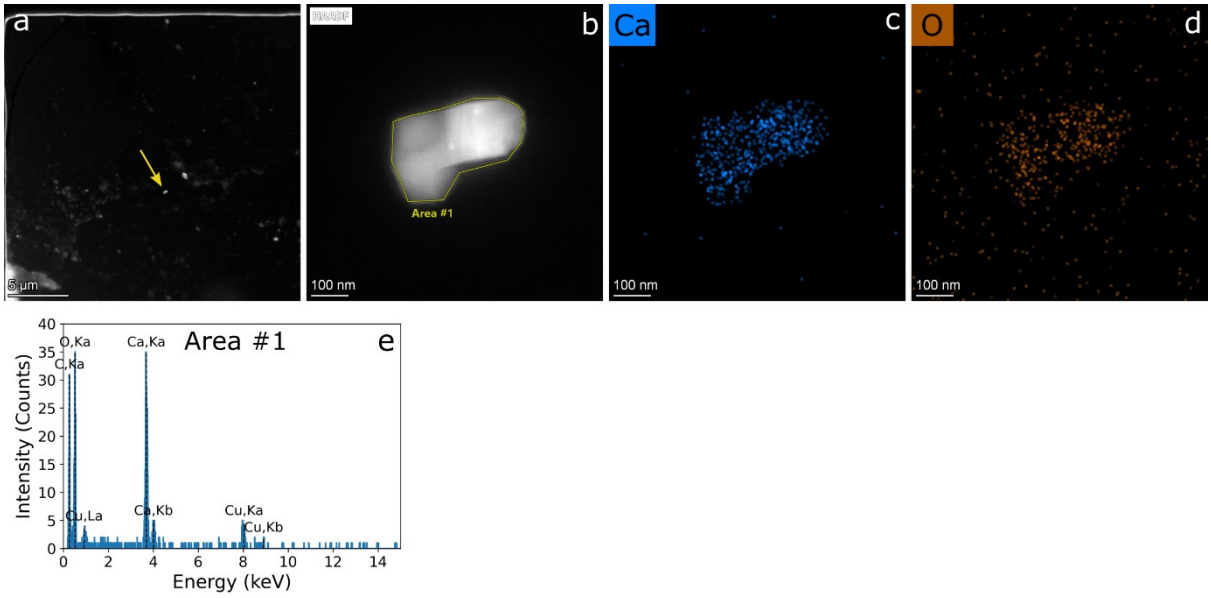

Figure 19. Low magnification HAADF-STEM image of particles (a). High magnification HAADF-STEM image of the particle indicated by the yellow arrow (b). EDX analysis shows that the particle contains Ca and O, with the spectral image of Ca (c) and O (d), and the EDX spectrum of the area #1 (e), as indicated in b.

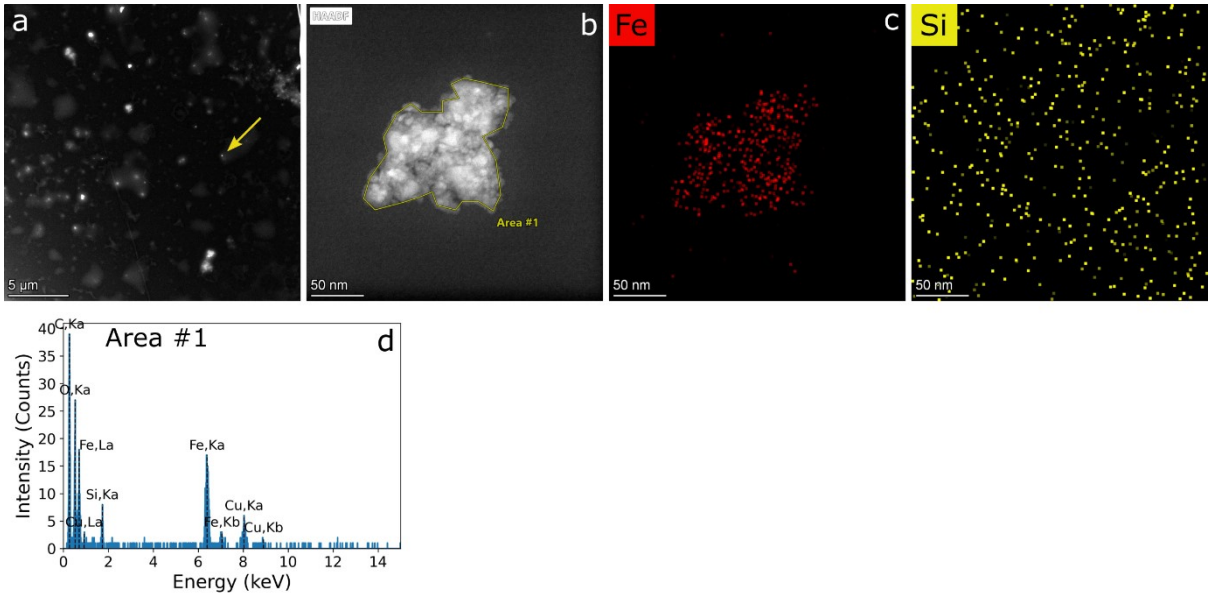

Figure 20. Low magnification HAADF-STEM image of particles (a). High magnification HAADF-STEM image of the particle indicated by the yellow arrow (b). EDX analysis shows that the particle contains Fe, while Si is present as a background only, with the spectral image of Fe (c) and Si (d), and the EDX spectrum of the area #1 (e), as indicated in b.

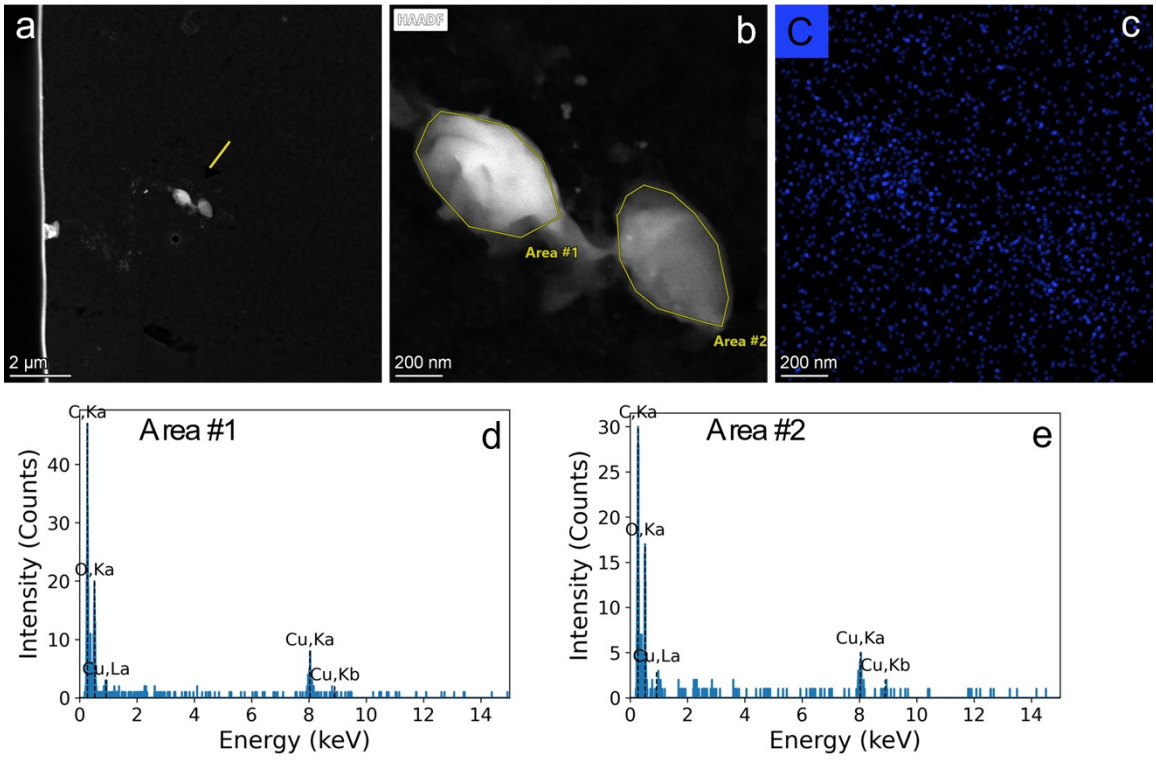

Figure 21. Low magnification HAADF-STEM image of particles (a). High magnification HAADF-STEM image of the particles indicated by the yellow arrow (b). EDX analysis shows that both particles contain a slightly elevated C content compared to the background, with the spectral image of C (c) and the EDX spectrum of the area #1 (d) and area#2 (e), as indicated in b.

3. Drop-on-grid deposition + evaporation (overnight)

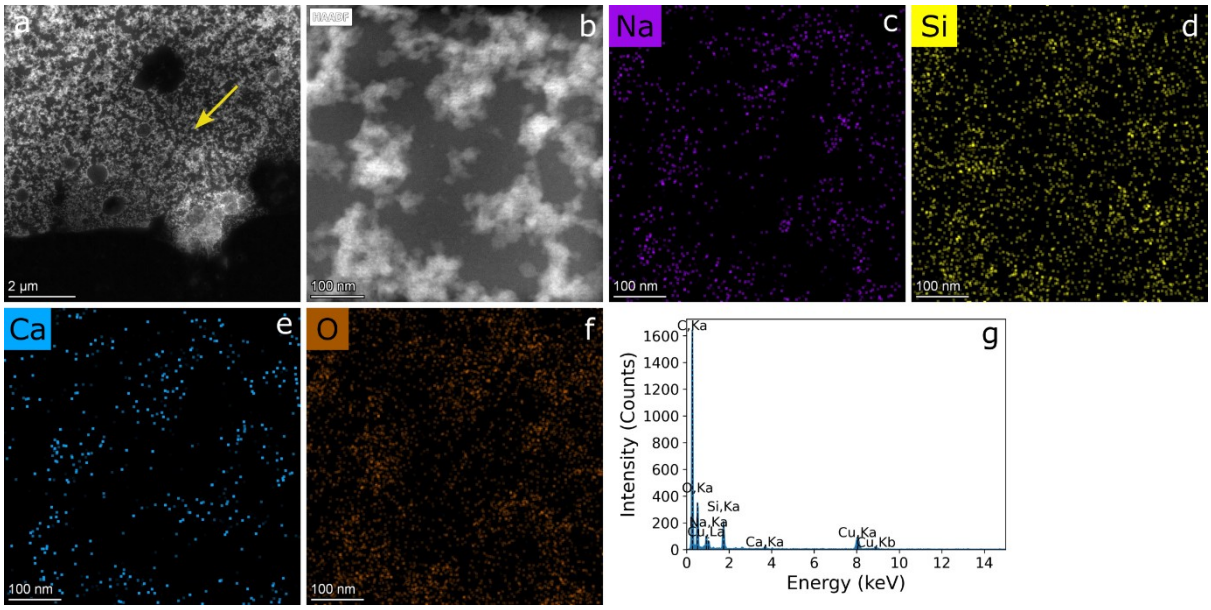

Figure 22. Low magnification HAADF-STEM image of very densely deposited particles (a). High magnification HAADF-STEM image of the particles in the region indicated by the yellow arrow (b). EDX analysis shows that the particles contain Na, Si, Ca and O, with the spectral image of Na (c), Si (d), Ca (e) and O (f) and the EDX spectrum of the image b (g).

G. TEM and STEM with EDX by University of Parma

For the PS suspension, sizing was performed on approximately 200 nanoparticles using ImageJ software, yielding a mean particle diameter of 195±6 nm compared to the certified value of 202±4 nm. Representative images are shown below.

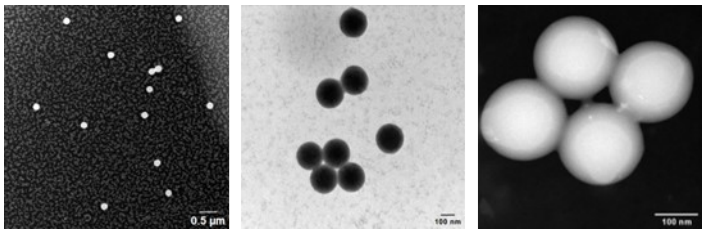

Figure 23. Representative TEM images of PS particles.

Regarding nanoPP solution in all the sample preparations tested, TEM and STEM imaging revealed the presence of isolated nanoparticles as well as irregular aggregates, as shown in the figure below. Particle sizing, performed on approximately 250 nanoparticles using ImageJ software, yielded a mean particle diameter of 92±37 nm, with most particles (63%) falling within the 70–120 nm range.

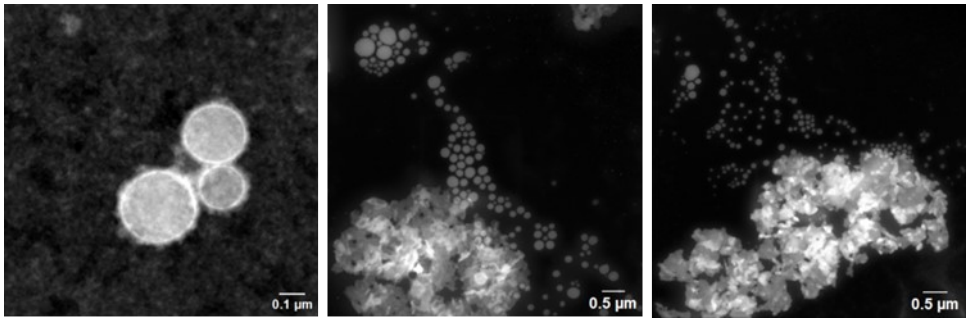

Figure 24. Representative TEM images of nanoPP.

This size was consistent with nanoparticles, although the EDX spectra acquired on selected particles revealed the presence of multiple elements, including Ca and O, in addition to the C signal (as shown below). In the case of aggregates, further elements such as Na, Si and Cl were also detected. Analysis of blank samples revealed comparable levels of Na and O, as well as low levels of Ca, Si and Cl. Due to the presence of these additional elements, it is not possible to unambiguously identify the particles as nanoPP.

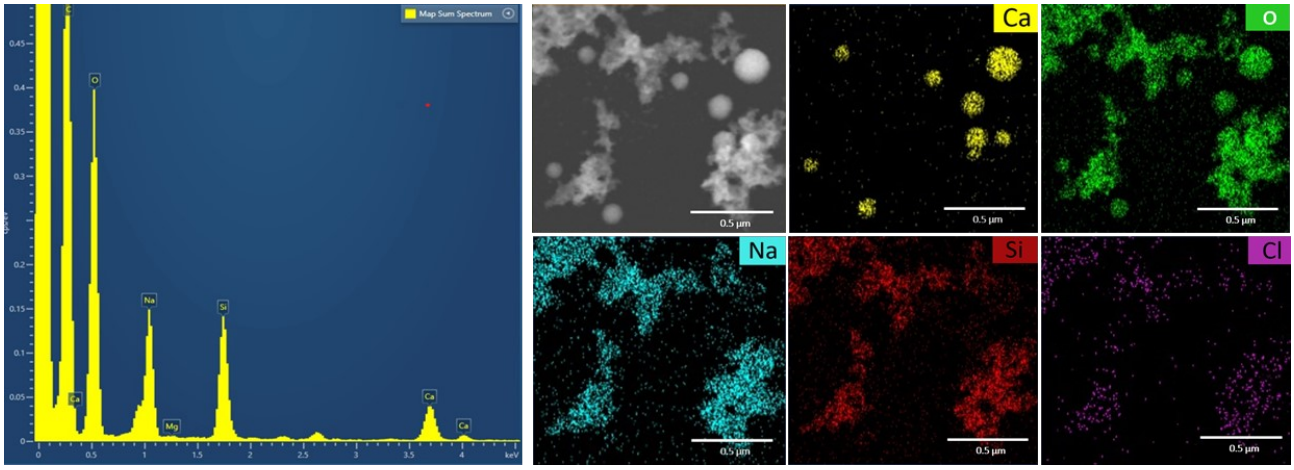

Figure 25. EDX spectra and maps of nanoPP.

H. AFM Results by SMD

The preferred deposition method of sample on substrate is blow-drying after incubation. This is performed on freshly cleaved mica substrate, with pre-coating of the substrate by poly-L-lysine, if needed. The sample is blow dried with nitrogen before measurement. This avoids “coffee ring stain” drop drying effect. (citation: 10.1007/978-1-60327-198-1_7).

Figure below presents the results, with one AFM image and the size distribution NanoPP sample obtained from several images, with maximum height as measurand for the size. The images reveal the presence of particles, brought by a solution leaving very small droplets of dried solute around. Nevertheless, image processing makes possible. However, deposition is quite sparse, even if the deposition is already optimized.

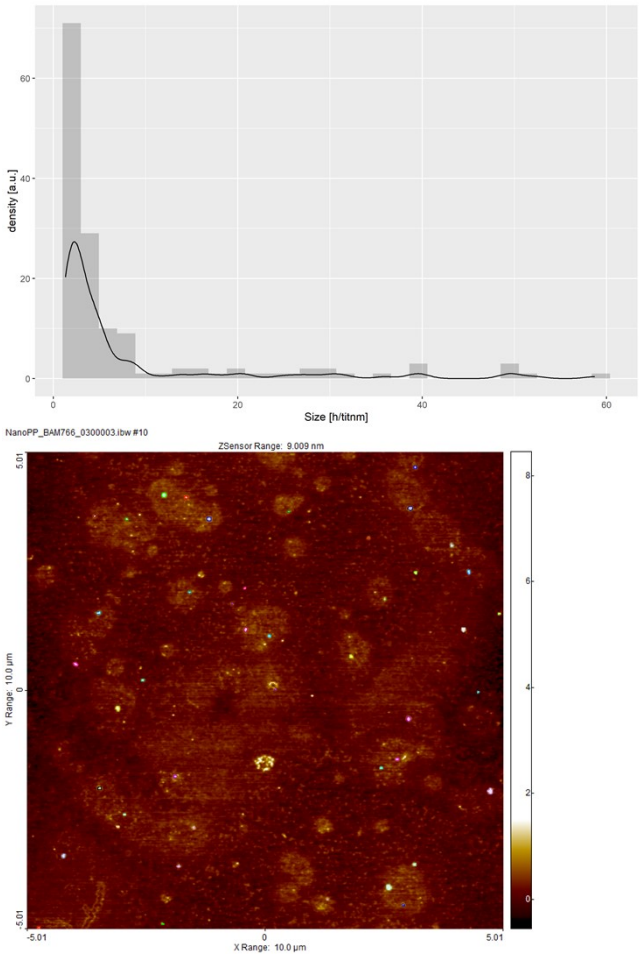

Figure 26. AFM images and corresponding size distribution of nanoPP.

Other deposition methods have been investigated but with less success. Glass substrates (cleaned microscopy slides) show a rugosity of 10 nm which is bigger than for mica (<1 nm), causing potential hindrance of smaller part of the population. Drop drying promotes patterned agglomeration. Drop drying in an alcohol saturated environment (evaporation could slightly dissolve the exterior layers of the particles, as has been observed on polystyrene beads of small size). For AFM measurement, the most direct and accurate size measurand is the height, metrologically speaking. For indication, the area equivalent diameter is also given for qualitative comparison It can only be used qualitatively

because of the high impact of the tip convolution artefact, and of image processing possible biases (influence of the height treshold to delinate the particles). The vertical vs lateral aspect ratio is however clearly significant, indicating a flake like particle shape.

Table 11. Summary of the results obtained with AFM.

Number of particles	Average maximum height h [nm] (k=1)	D10/d50/d90 [nm]	Average equivalent diameter [nm] (k=1)	D10/d50/d90 [nm]
145	8.07+- 0.98	1.8/3.1/25	110+-9.1	1.56/66.4/207

For comparison with other labs, drop drying deposition method has been attempted. However, the pictures revealed of coffee stain, even in the case of deposition of a small volume (10 µL, where 25 µL is the usual volume for 9 mm mica disks) and were not considered fit-for-purpose.

I. Raman analysis of the nanoPP

Table 12. Assignments of the peaks of nanoPP Raman spectrum.

	Assignment
a	$\nu_a CH_3$
b	$\nu_a CH_2$
c	νCH
d	$\nu_s CH_2$
e	$\nu_s CH_3$
f	$\nu_s CH_2$
g	$\delta_a CH_3$, δCH_2
h	$\delta_a CH_3$
i	$\delta_s CH_3$
j	δCH
k	τCH_2, δCH, νCC_b
l	νCC_b, ρCH_3, δCH
m	νCC_b, $\nu C\text{-}CH_3$, δCH, ρCH_3
n	$\nu C\text{-}CH_3$, νCC_b, δCH
o	ρCH_3, δCH, wCH_2
p	ρCH_3, νCC_b
q	ρCH_3, νCC_b
r	ρCH_3, ρCH_2, δCH
s	ρCH_2, νCC_b, $\nu C\text{-}CH_3$, ρCH_3
t	ρCH_2, νCC_b, $\nu C\text{-}CH_3$

Repeatability of Raman analysis - Raman spectra of 10 different vials of nanoPP collected by INRiM:

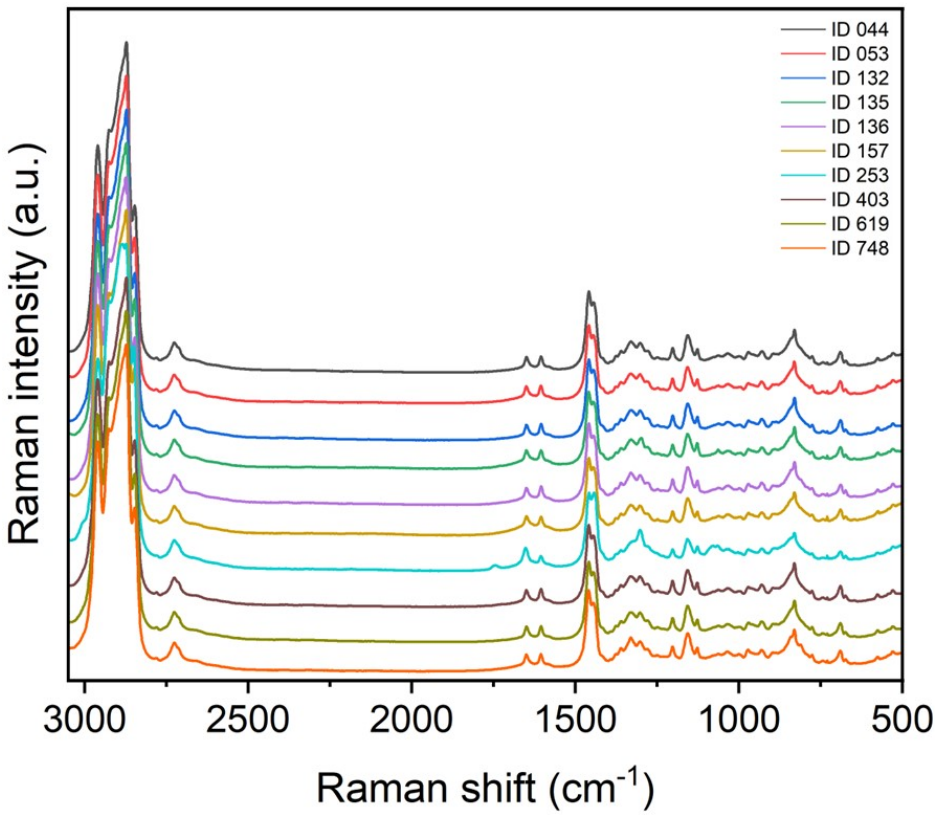

Figure 27. Repeatability of Raman analysis.

The nanoPP suspension was also analysed by Raman by LNE. A drop was deposit on a silicon wafer to make an agglomerate at the surface a spectrum was made on the total amount deposit) to access to the global chemistry (*Note: Chemical analysis of individual particles by Raman at nanoscale cannot be performed due to lower size limit of detection*).

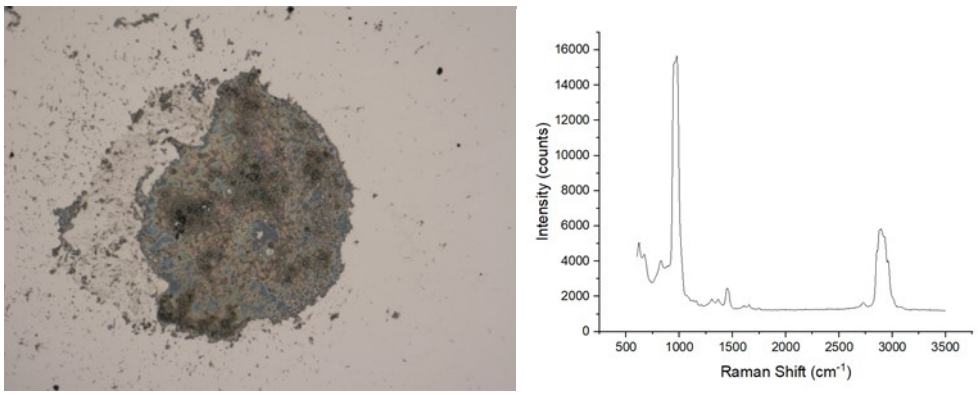

Figure 28. SEM image of the nanoPP deposition and a corresponding Raman spectra.

J. Ion chromatograms of the polypropylene calibration standard and the nanoPP

PP Co-polymer calibration standard

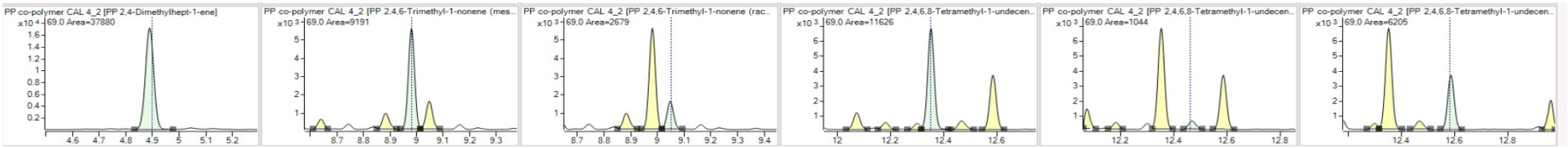

nanoPP stock

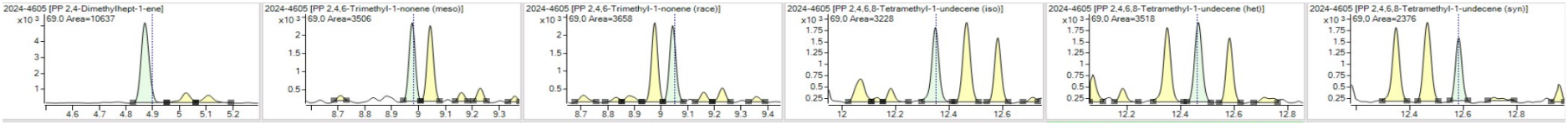

Figure 29. Ion chromatograms of the polypropylene calibration standard and the nanoPP.

Extracted ion chromatogams of the polyproplyene (PP) co polymer calibration standard (top) and the nanoPP test material (bottom). Individual graphs show the chromatographic region for the individual pyrolysis peak markers (L-R): 2,4-dimethylhept-1-ene (m/z 70 and 126), 2,4,6-trimethyl-1-nonene (meso) and 2,4,6-trimethyl-1-nonene (racemic) (m/z 69 and 97), 2,4,6,8-tetramethyl-1-undecene (isotactic), 2,4,6,8-tetramethyl-1-undecene (heterotactic) and 2,4,6,8-tetramethyl-1-undecene (syntactic) (m/z 69 and 111).